POROUS IMMERSED BOUNDARIES

by

Badri Ratnam
MS in Mechanical Engineering, University of South Florida, 2000

A PROJECT SUBMITTED IN PARTIAL FULFILLMENT
OF THE REQUIREMENTS FOR THE DEGREE OF
MASTER OF SCIENCE
in the Department
of
Mathematics

SIMON FRASER UNIVERSITY
Fall 2008

APPROVAL

Name: Badri Ratnam

Degree: Master of Science

Title of project: Porous Immersed Boundaries

Examining Committee: Dr. Razvan C. Fetecau
Chair

Dr. John Stockie,
Associate Professor, Mathematics
Simon Fraser University
Senior Supervisor

Dr. Mary-Catherine Kropinski,
Associate Professor, Mathematics
Simon Fraser University
Committee member

Dr. David J. Muraki,
Associate Professor, Mathematics
Simon Fraser University
Internal Examiner

Date Approved: December 2, 2008

Abstract

We describe a generalization of the immersed boundary (IB) method for simulating fluid-structure interaction, which incorporates the effect of porosity into elastic immersed boundaries. The mathematical formulation of the IB problem can be altered to allow for porous leakage by incorporating an additional porous slip velocity term in the membrane evolution equation. We study how this change affects the linear stability of the underlying governing equations, comparing to previously published results for an impermeable membrane. We also address the impact of membrane permeability on numerical computations through a study of stability and time step restrictions for certain discrete formulations of the IB problem. All IB computations are characterized by an inherent volume loss which resembles a porous membrane leaking fluid – we obtain an estimate of this "inherent membrane permeability" and use it to devise a method for reducing the volume loss in computations. We perform a series of IB simulations to confirm the validity of our approach.

Acknowledgments

I owe heartfelt appreciation to many for their support and guidance that made this project possible. First, I would like to thank my advisor, Dr. John Stockie for his support during this effort. With his guidance, I learnt how to approach physical problems from a mathematical perspective. I have often tapped into his intricate knowledge of the immersed boundary method and computational fluid dynamics (CFD) during the course of this work. John's support was instrumental in making possible my visit to Fraunhofer Institut Techno- und Wirtschaftsmathematik (ITWM), a highly rated industrial mathematics institute in Kaiserslautern, Germany to further my research.

I am grateful to my advisory committee member, Dr. Mary Catherine Kropinski and internal examiner, Dr. David J. Muraki for taking the time to review my work.

I thank the faculty members in the Department of Mathematics, Simon Fraser University who, through courses, seminars and discussions increased my interest and knowledge of applied mathematics.

Special thanks to fellow graduate student Bryan Quaife, who took the time to review my work and share feedback. Many thanks to the other applied math graduate students who made my graduate experience special.

I'm grateful to my family, especially my parents and parents-in-law for their constant support and encouragement.

Above all, I would like to thank my best friend and confidant, my wife, Poornima Padmanabhan. Without her, this effort would not have been possible. She was always there for help, advice, support, and laughter. She has been and will be the vital pillar of my life.

Contents

List of Tables

List of Figures

Chapter 1

Introduction

1.1 Overview

In his seminal paper [25], Peskin introduced the immersed boundary method (IBM) to simulate flow patterns around heart valves. Over the decades, the IBM has evolved as a robust approach for simulating the hydrodynamic coupling between the fluid and elastic membrane. The IBM has attracted considerable interest from mathematicians, scientists and engineers alike. It has been used to simulate engineering phenomena such as flapping aircraft wings [10], flow inside an internal combustion engine [33], and flapping filaments in soap films [34]. The IBM has also been used to simulate biological phenomena such as blood flow in the heart [17], swimming organisms [4], platelet aggregation [9] and wave propagation in the inner ear [2]. From a mathematical perspective, this problem has attracted considerable attention on account of the challenges: sensitivity to small perturbations, singularity formation, topological changes and severe time stepping constraints due to high stiffness [12].

The numerical method as originally proposed by Peskin has several advantages: simplicity, geometric flexibility and it is easily vectorisable. It also suffers from several deficiencies: it is only first order accurate, it is very stiff and it is limited to low Reynolds numbers flows [32]. Many algorithmic improvements have been suggested in recent years that address these problems, in particular semi-implicit methods that partially alleviate the stiffness [23], adaptive refinement [11] to increase accuracy, and high order upwinding schemes to loosen Reynolds number restrictions [18, 11].

The immersed boundary (IB) or "membrane" in the standard IBM is impermeable i.e.no

fluid leakage is allowed through the membrane [1]. Porous immersed structures exist in biological systems such as artery walls [13], brain tissue [28], lipid vesicles [14] and in engineering applications such as ocean wave barriers [3, 15]. The IBM could conceivably be used to simulate such phenomena and some attempts have been made to incorporate porosity into the IBM [16, 20, 8].

In this work, we will develop a generalization the IBM based on [16] to allow porous flow across the membrane driven by the fluid pressure gradient[2]. To this end, we will compare our simulations with an analytical solution, study the effects of porosity on stability both of the analytical solution and numerical discretization. We will also introduce a new technique to reduce volume loss.

1.2 Outline

In Chapter 2, we will describe the non-porous and porous IBM, and provide a complete mathematical formulation. We will obtain an analytical solution for a porous circular membrane and compare the analytical solution with numerical simulations.

In Chapter 3, we will study the effect of porosity on stability. We will do four different types of stability analysis: 1D linear stability, 1D semi-discrete analysis, 1D fully discrete analysis and 2D linear stability analysis of a circular fiber and compare our results with numerical simulations where possible.

In Chapter 4, we will introduce a new technique to reduce volume loss and describe its effect on stability. We will also show why volume loss resembles porous flow driven by Darcy's law.

In Chapter 5, we will briefly outline the conclusions of our research and future directions.

[1] Some unintentional leakage known as 'volume loss' does occur on account of numerical errors and this is the subject of Chapter 4.

[2] This pressure gradient occurs on account of the IB force. It is not the same as osmotic pressure gradient.

Chapter 2

Porous Immersed Boundary Method

2.1 Introduction

Some recent efforts have been made to generalize the IBM for porous flow. Kim and Peskin [16] modeled air vents in a canopy of a parachute by deliberately violating the no slip condition between the fiber and fluid and introducing a porous slip velocity. Stockie [30] built on Kim and Peskin's approach to simulate porous flow based on Darcy's law. He also used this formulation to create a new method for reducing volume loss. Layton [20] introduced a normal slip velocity in the closely related immersed interface method (IIM) to simulate porous flow driven by transmural water pressure *and* solute concentration. Fauci and Dillon [8] study flow through granular media at the pore scale by treating grains as immersed boundaries.

In this work, we will follow and extend the work of Kim and Peskin [16] and Stockie [30] to simulate porous flow. We will begin by describing the non-porous IBM and then show how we can incorporate porosity by means of a porous slip velocity. We will obtain an analytical solution for a model presented in [16] and show that our numerical results agree with the analytical solution.

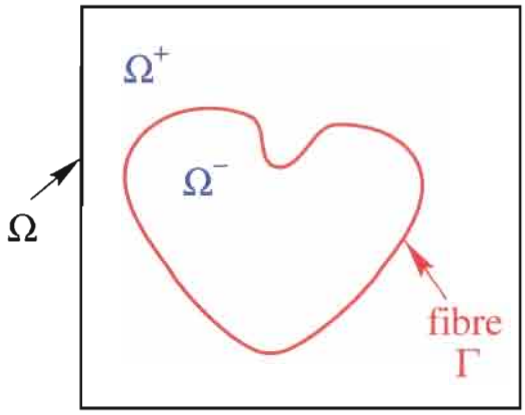

Figure 2.1: The fluid domain and fiber

2.2 Mathematical Formulation of the Non-porous Problem

We will present the governing equations of the IBM following the notation used by Stockie [30] and Peskin [27]. Figure 2.1 shows a two dimensional fluid domain Ω with a IB described by a continuous non-intersecting curve Γ. Let $\vec{x} = (x, y)$ be the Eulerian grid and $\vec{u}(\vec{x}, t)$ (cm/s) be the Eulerian velocities at time t. Let the pressure be $p(\vec{x}, t)$ (g/cms^2). Let the density and dynamic viscosity be ρ (g/cm^3) and μ (g/cms^2) respectively. The incompressible Navier-Stokes equations are

$$\rho(\vec{u} + \vec{u} \cdot \nabla\vec{u}) = \mu\Delta\vec{u} - \nabla p + \vec{f} \tag{2.1}$$

$$\nabla \cdot \vec{u} = 0. \tag{2.2}$$

Let $\vec{f}(\vec{x}, t)$ (g/cm^2s^2) be the force exerted by the IB per unit volume of fluid. The immersed fiber is on a Lagrangian grid. Let $\vec{X}(s, t) = (X(s, t), Y(s, t))$ be the Lagrangian velocities at time t, where s is a parametrization of the membrane geometry in some reference configuration. The fluid force may be written as

$$\vec{f}(\vec{x}, t) = \int_\Gamma \vec{F}(s, t)\delta(\vec{x} - \vec{X}(s, t))ds \tag{2.3}$$

where $\delta(\vec{x})$ is the two-dimensional delta function (see Section 2.6). The function $\vec{F}$ (g/s^2) is the IB force per unit length (also known as the fiber force density). To determine $\vec{F}$ we assume that the fiber force only acts in the direction of the fiber and that the fiber has no bending or torsional resistance. Using the notation of [32], the fiber force may be written

as

$$\vec{F} = \frac{\partial}{\partial s}(T\vec{\tau}) \tag{2.4}$$

where the fiber tension T takes the form

$$T = \sigma\left(\left|\frac{\partial \vec{X}}{\partial s}\right| - L\right) \tag{2.5}$$

where L is the resting length, $\sigma(g/cms^2)$ is the spring constant and $|\frac{\partial \vec{X}}{\partial s}|$ is the fiber strain. The unit tangential vector is

$$\vec{\tau} := \frac{\frac{\partial \vec{X}}{\partial s}}{|\frac{\partial \vec{X}}{\partial s}|}.$$

Hence, the force density is

$$\vec{F}(s,t) = \sigma\frac{\partial}{\partial s}\left[\frac{\partial \vec{X}}{\partial s}\left(1 - \frac{L}{|\frac{\partial \vec{X}}{\partial s}|}\right)\right]. \tag{2.6}$$

For a fiber with zero resting length, we get $\vec{F} = \sigma\vec{X}_{ss}$. For a non-porous IB, there should be no slip i.e. the fiber must move with the same velocity as the neighboring fluid particles

$$\vec{X}_t = \vec{u}(\vec{X}(s,t)) \tag{2.7}$$

which can be written in terms of a delta function convolution as

$$\vec{X}_t = \int_\Omega \vec{u}(\vec{x},t)\delta(\vec{x} - \vec{X}(s,t))d\vec{x}. \tag{2.8}$$

Eqs. (2.8) and (2.3) together with (2.1) and (2.2) are known as the delta function formulation of the immersed fiber problem. To incorporate porosity, we will introduce a porous slip velocity term in (2.8) later in Section 2.4.

2.3 Jump Formulation

We will describe an alternate and equivalent formulation known as the jump formulation. In this formulation, (2.1) and (2.2) will remain the same. The no slip condition (2.7) will be used instead of (2.8) to avoid use of delta functions. Instead of using the delta function to interpolate the force and fluid parameters, the jump conditions give the 'jump' in pressure

and velocities across the interface. The following relations will be in the place of (2.8) and (2.3)

$$[\vec{u}] = 0 \tag{2.9}$$

$$\mu\tau \cdot [n \cdot \nabla\vec{u}] = -\frac{\vec{F} \cdot \vec{\tau}}{|\vec{X}_s|} \tag{2.10}$$

$$[p] = \frac{\vec{F} \cdot \vec{n}}{|\vec{X}_s|} \tag{2.11}$$

where $[.] = (.)|_{\Gamma+} - (.)|_{\Gamma-}$ denotes the difference in a quantity on either side of the fiber and $\vec{n}$ is the unit normal vector where $\vec{n} \cdot \vec{\tau} = 0$. Eq. (2.9) comes from $\vec{u}$ being continuous across Γ. Eqs. (2.10) and (2.11) come from integrating the momentum equations across Γ, and a derivation of the jump conditions is given in [24].

2.4 Introducing Porosity

We follow Kim and Peskin [16], who modeled air vents in a parachute canopy "by allowing the normal velocity of the canopy to differ from that of the nearby fluid by an amount proportional to the normal component of the boundary force". They derive the porous slip velocity in Section K2[1]. Eq. (K15) gives us an expression for porous slip velocity. Changing (2.8) based on (K15), we get

$$\vec{X}_t = \int_\Omega \vec{u}(\vec{x}, t)\delta(\vec{x} - \vec{X}(s, t))d\vec{x} - U_s\vec{n} \tag{2.12}$$

where U_s is the *porous slip velocity* given by

$$U_s = -\alpha\frac{\vec{F} \cdot \vec{n}}{|\vec{X}_s|^2}. \tag{2.13}$$

which can be interpreted as a *porous conductance* α with units cm^2s/g. In the non-porous IBM, there is a no slip condition between the IB and the surrounding fluid. The porous flux, driven by Darcy's law is directed purely in the normal direction to the IB and is driven by pressure difference from one side to the other. Hence, we introduce the porous slip velocity U_s to violate the no slip condition only in the normal direction [30, 16]. The tangential no

[1]We will number sections and equations from paper [16] with a prefix K.

slip condition still holds. We have used α to represent the constant $\beta\gamma$ in the form of [16]. In a general setting, we hypothesize α has the following form

$$\alpha = \frac{K(|\vec{X}_s|)}{\mu M_r(|\vec{X}_s|)}$$

where K and M_r are the permeability and membrane porous resistance respectively. K and M_r are functions of $|X_s|$ because as the fiber extends the number of pores should increase and so should the permeability [24]. The exact relationship of α to $|X_s|$ will depend on the porous properties of the membrane. However, for the sake of simplicity, we have assumed α to be a constant. Using (2.11), (2.13) can be rewritten to be consistent with Darcy's law for porous flow

$$U_s = -\frac{K_e}{\mu a}[p] \tag{2.14}$$

where K_e is the permeability of the IB with units cm^2 and a is the thickness of the porous region, and $K_e = \frac{\alpha\mu a}{|\vec{X}_s|}$ for consistency.

2.5 Solution Algorithm

We will present the "FE/ADI" (forward Euler, alternating direction implicit) solution algorithm following the outline of [30], where we discretize advection and diffusion terms implicitly using ADI and other terms explicitly using FE. The solution algorithm is a mixed Eulerian-Lagrangian approach, where the fluid variables are approximated on a Cartesian grid and the membrane Variables are on a moving set of Lagrangian points. The fluid domain ($\Omega = [0, L] \times [0, L]$) is discretized as a $N \times N$ grid, where $h = \frac{L}{N}$ is the grid spacing. The membrane variables are discretized at a set of N_b points which move relative to the fluid grid and are parametrized by $s_l = lh_b$, where h_b is the fiber spacing. The time domain $[0, T]$ is divided into M sub-intervals, where $k = \frac{T}{M}$ is the timestep. The variables $\vec{u}^n_{i,j}$, $\vec{p}^n_{i,j}$ and $\vec{f}^n_{i,j}$ are the discrete fluid velocity, pressure and force respectively at $x_i = ih, y_j = jh$ for $i, j = 1, 2, \ldots N$ and $t_n = nk$ for $n = 1, 2, \ldots M$. $\vec{F}^n_l$ and $\vec{X}^n_l$ are respectively the fiber force density and fiber position on the Lagrangian grid respectively at time t_n and position $\vec{X}_l$ for $l = 1, 2, ...N_b$. We will use the cosine delta function outlined in Section 2.6. We will assume that at the nth timestep we have the boundary position $\vec{X}^{n-1}_l$ and fluid velocity $\vec{u}^{n-1}_{i,j}$ from the previous step. We will assume periodic boundary conditions on Ω and that Γ is a closed curve. We begin with initial conditions for $\vec{u}$ and $\vec{X}$ at timestep $n = 0$.

1. Calculate the fiber force density $\vec{F}_l^n$ based on X_l^n using centered differences on (2.6).

2. Spread the fiber force density onto nearby fluid points using the following discretization of (2.3)

$$\vec{f}_{i,j} = h_b \sum_l \vec{F}_l^n \delta_h(x_i - X_l^{n-1}) \delta_h(y_j - Y_l^{n-1}).$$

where $\delta_h(x)$ is the delta function approximation.

3. Solve the Navier Stokes Equations using Chorin's split-step projection scheme:

   (a) Update the velocity components $\vec{u}_{i,j} = (u_{i,j}, v_{i,j})$ by using the convective, viscous and forcing terms using alternating direction implicit approach and standard centered differences to approximate all derivatives.

$$\vec{u}_{i,j}^{n,0} = \vec{u}_{i,j}^{n-1} + \frac{k}{\rho}\vec{F}_{i,j}^n,$$

$$\begin{aligned}
\vec{u}_{i,j}^{n,1} + \frac{k}{2h}u_{i,j}^{n-1}(\vec{u}_{i+1,j}^{n,1} - \vec{u}_{i-1,j}^{n,1}) - \frac{\mu k}{\rho h^2}(\vec{u}_{i+1,j}^{n,1} - 2\vec{u}_{i,j}^{n,1} + \vec{u}_{i-1,j}^{n,1}) &= \vec{u}_{i,j}^{n,0}, \\
\vec{u}_{i,j}^{n,2} + \frac{k}{2h}v_{i,j}^{n-1}(\vec{u}_{i+1,j}^{n,2} - \vec{u}_{i-1,j}^{n,2}) - \frac{\mu k}{\rho h^2}(\vec{u}_{i+1,j}^{n,2} - 2\vec{u}_{i,j}^{n,2} + \vec{u}_{i-1,j}^{n,2}) &= \vec{u}_{i,j}^{n,1}
\end{aligned}$$

   The last two equations can be written as tridiagonal systems.

   (b) Project the velocity onto the space of divergence-free vector fields by first solving the Poisson equation for the pressure $p_{i,j}^n$

$$p_{i+2,j}^n + p_{i-2,j}^n + p_{i,j-2}^n + p_{i,j+2}^n - 4p_{i,j}^n = \frac{2\rho h}{k}(u_{i+2,j}^{n,2} - u_{i-1,j}^{n,2} + v_{i,j+1}^{n,2} - v_{i,j-1}^{n,2})$$

   which is a periodic pentadiagonal linear system that can be solved most efficiently using a Fast Fourier Transform (FFT).

   (c) The velocity is updated to enforce the divergence free condition.

$$\vec{u}_{i,j}^n = \vec{u}_{i,j}^{n,2} - \frac{k}{2\rho h}(p_{i+1,j}^n - p_{i-1,j}^n, p_{i,j+1}^n - p_{i,j-1}^n)$$

4. Find the new fiber position using (2.12).

$$\vec{X}_l^n = \vec{X}_l^{n-1} + \frac{4\alpha k h_b^2 (\vec{F}_l^n . \vec{n}_l^{n-1})}{|\vec{X}_{l+1}^{n-1} - \vec{X}_{l-1}^{n-1}|^2} + kh^2 \sum_{i,j} \vec{u}_{i,j}^n \delta_h(x_i - X_l^{n-1}) \delta_h(y_i - Y_l^{n-1})$$

5. Increment n and go to step 1.

2.6 Delta Functions

The delta function formulation of the IBM is so named because it couples the fluid and fiber equations together by means of a delta function ((2.8) and (2.3)). In the IBM, the force is zero everywhere except on the fiber. Hence, the fluid force can be regarded as a distribution and can be written as a convolution of the fiber force with the delta function [32]. The fiber force is thus interpolated onto the fluid grid. Similarly, the delta function is also used to transfer the fluid velocities onto the fiber grid. $\vec{U}(X,Y)$ is a simple finite difference approximation of the integral in (2.8) and is given by

$$\vec{U}(X,Y) = \sum_{\vec{x}\in Z_h^2} \vec{u}(x,y)\delta_h(x-X)\delta_h(y-Y)h^2$$

where the set of finite difference grid points are represented by

$$\begin{aligned} Z_h^2 &= Z_h \times Z_h \\ Z_h &= \{x : x = ih,\ y : y = jh\}. \end{aligned}$$

Peskin [27, 26] has a list of discrete compatibility conditions that should be satisfied by the delta function. Some properties [24] of the delta function $\delta_h(x)$ are

$$\begin{aligned} \delta_h(x) &= 0 \text{ for } |x| > O(h) \\ \delta_h(x) &= O(h^{-1}) \\ \delta_h'(x) &= O(h^{-2}) \\ \sum_{x\in Z_h^2} \delta_h(x-X) &= 1 \qquad (2.15) \\ \sum_{x\in Z_h^2} (x-X)\delta_h(x-X)h &= 0 \qquad (2.16) \\ \sum_{x\in Z_h^2} (x-X)^2\delta_h(x-X)h &= Ch^2. \qquad (2.17) \end{aligned}$$

The most commonly used delta function in IB literature (which we will use in our simulations) is

$$d_h = \delta_h(x)\delta_h(y)$$

$$\delta_h(x) = \begin{cases} \frac{1}{4h}(1+\cos(\frac{\pi x}{2h})) & |x| \le 2h \\ 0 & |x| > 2h. \end{cases} \qquad (2.18)$$

This delta function satisfies all the compatibility conditions except for the first moment condition (2.16). By changing the spatial discretization h in (2.17), we find that $C = 0.5$ for the chosen delta function (2.18).

2.7 Analytical Solution

We will derive an analytical solution to the porous IB problem for a circular membrane. We will follow the derivation given in [30]. In [30], the slip velocity looks like $-\alpha\frac{\vec{F}\cdot\vec{n}}{|\vec{X}_s|}$, i.e. our slip velocity (2.13) has an extra $|\vec{X}_s|$ term in the denominator. Hence, our model is slightly different because we have incorporated the effect of membrane compression/stretching on porosity. Let the unstressed equilibrium state of the membrane be a circle of radius $R_{eq} \geq 0$ and let Let R_0 be the initial radius of the membrane. The membrane configuration can be written as

$$\vec{X}(s,t) = r(t)[\cos s, \sin s]$$

where $s \in [0, 2\pi]$ is the polar angle measured counter-clockwise. The other membrane quantities appearing in the IB equations are

$$\begin{aligned} \vec{X}_s &= r(t)[-\sin s, \cos s] \\ \vec{\tau} &= [-\sin s, \cos s] \\ |\vec{X}_s| &= r(t) \\ \vec{n} &= [\cos s, \sin s]. \end{aligned} \tag{2.19}$$

From (2.6), we get

$$\vec{F} = \sigma(R_{eq} - r(t))\vec{n}$$

and the porous slip velocity is given by

$$U_s = \frac{\alpha\sigma}{r(t)}(1 - \frac{R_{eq}}{r(t)}). \tag{2.20}$$

As in [30], we will assume that the contributions to dynamics from the underlying fluid flow are negligible, then the membrane motion is driven primarily by porous effects. Eq. (2.13) can be approximated $\frac{dr}{dt} \approx -U$. Then (2.20) becomes

$$\frac{dr}{dt} = -\frac{\alpha\sigma}{r(t)}(1 - \frac{R_{eq}}{r(t)}). \tag{2.21}$$

We will consider two cases.

Case 1, $R_{eq} = 0$

With zero resting length, we get the following solution when we integrate (2.21)

$$r(t) = \begin{cases} \sqrt{R_0^2 - 2\sigma\alpha t} & \text{if } R_0 \geq \sqrt{2\sigma\alpha t} \\ 0 & \text{otherwise.} \end{cases}$$

Figure 2.2 plots the numerical and analytical solutions for different values of α. The numerical solutions in this section have been corrected for volume loss. The parameters used in the simulation are given in Table 2.1. The analytical and numerical solution are very similar. To see the behavior of the solution over long times, we plot the numerical and analytical solution for the $\alpha = 10^{-4}$ case in Figure 2.3. The numerical and analytical solution match up very well till $t \approx 0.06$, when the solution goes unstable due to the CFL restriction (because of high fluid velocities).

Table 2.1: Parameters for numerical solution

radius of circle R	0.4
σ	10^4
ρ	1
μ	1
total time *tend*	0.02
timestep k	3.5×10^{-5}
mesh density	64×64
no. of fibers N	192
grid spacing h	0.0156
fiber spacing h_b	0.0103

Case 2, $R_{eq} > 0$

For this more general case($R_{eq} > 0$), we get the following solution when we integrate (2.21)

$$t = \frac{R_0^2 - r(t)^2}{2\sigma\alpha} + \frac{(R_0 - r(t))R_{eq}}{2\sigma\alpha} + \frac{R_{eq}^2}{\sigma\alpha} \ln\left(\frac{R_0 - R_{eq}}{R_0 - r(t)}\right).$$

Figure 2.4 plots the analytical and numerical solution for different values of α for the same parameters as above except that $R_{eq} = 0.1$. Once again, the analytical and numerical results are very similar. To see the behavior of the solution over long times, we plot the numerical and analytical solution for the $\alpha = 10^{-4}$ case in Figure 2.5. The numerical and analytical solution match up very well as long as the radius of the fiber is far greater than the resting

radius. As the solution approaches the resting radius, the solution diverges. The portion of the analytical solution below the resting radius ($R_{eq} = 0.1$) is not physical for initial radius greater than resting radius.

2.8 Choice of Parameters

In Table 2.2, we have listed the typical range of physical and numerical parameters used in IB computations

Table 2.2: Typical physical and numerical parameters

Parameter	Value or range
domain size	$1 - 5$
σ	$10^2 - 10^6$
ρ	1
μ	$0.04 - 1$
N	$32 - 256$
N_b	$128 - 384$
k	$10^{-6} - 10^{-3}$
α	$10^{-11} - 10^{-4}$

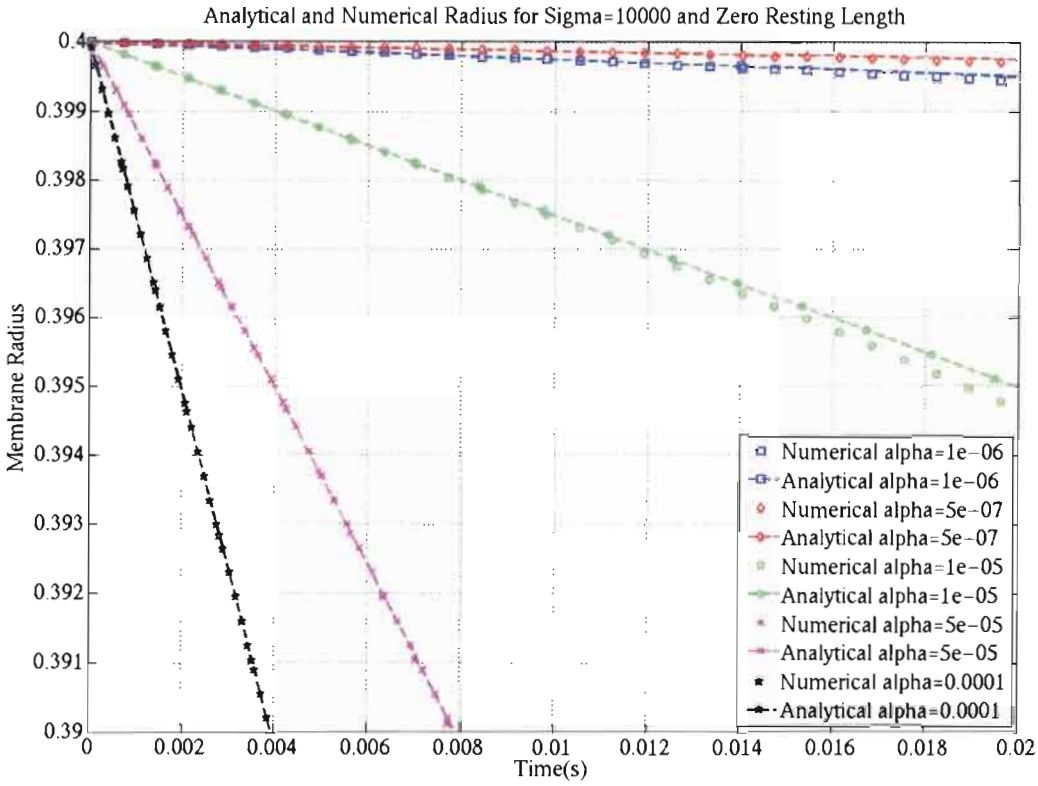

Figure 2.2: Analytical and numerical results for zero resting length

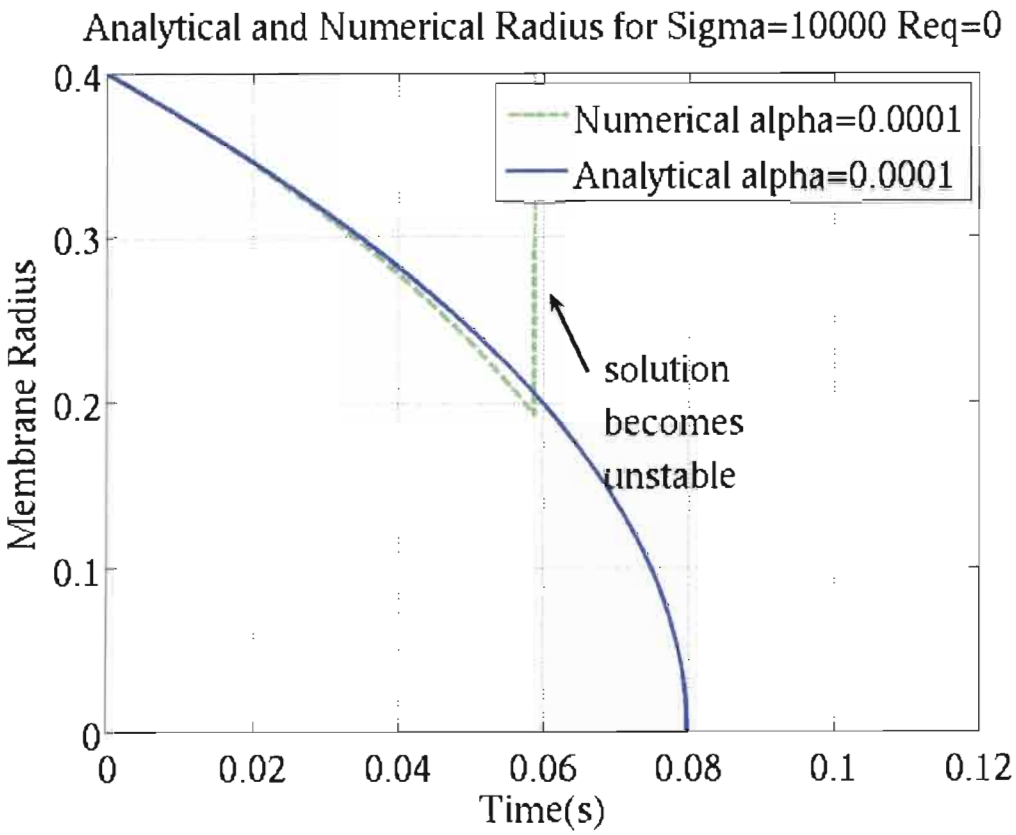

Figure 2.3: Analytical and numerical results over long time for zero resting length

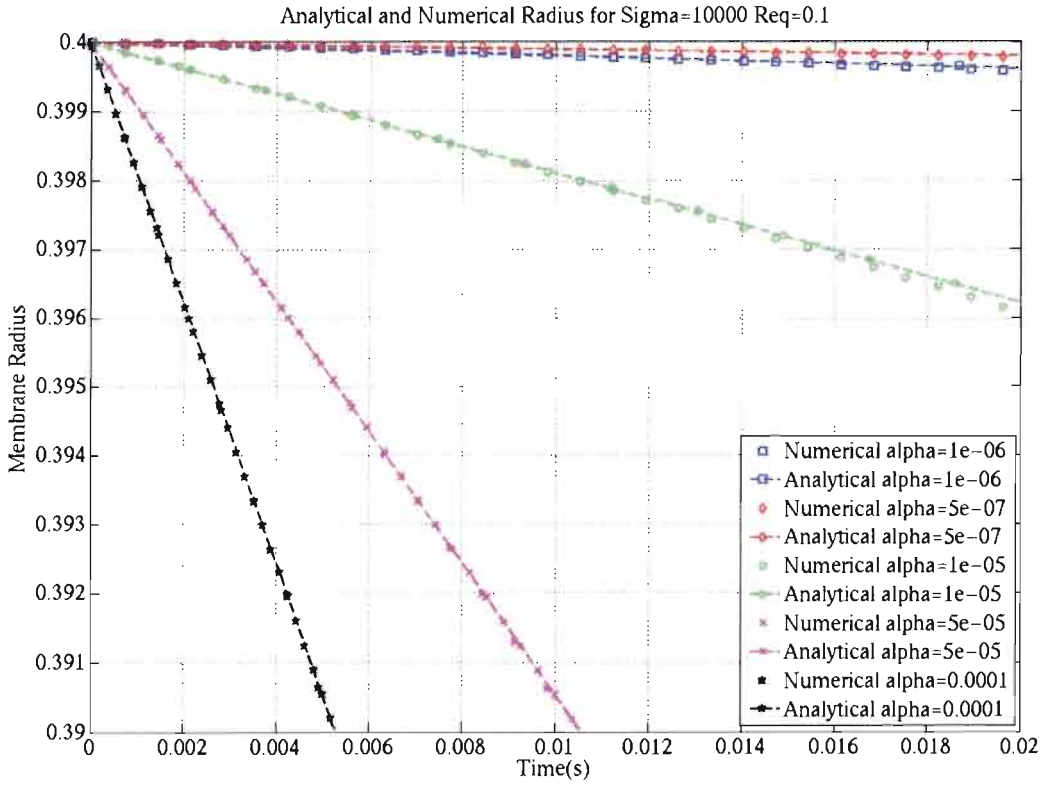

Figure 2.4: Analytical and numerical results for non-zero resting length

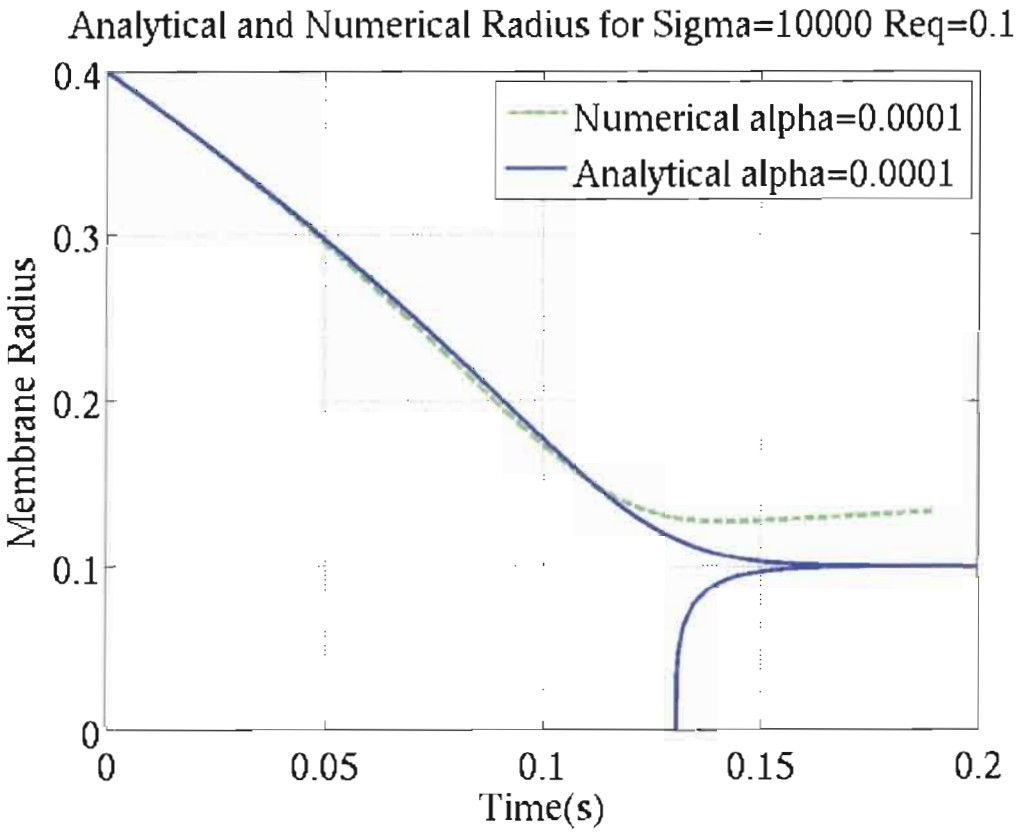

Figure 2.5: Analytical and numerical results over long time for non-zero resting length

Chapter 3

Stability

3.1 Introduction

In the previous chapter, we described a generalization of the IBM that allows porous flow driven by pressure difference across the IB. In this chapter, we will study how introducing this porosity will affect the stability of the IBM both in terms of the fully continuous and time discrete formulations. We will also derive a suitable timestep that we can use in our simulations. Stability of the IBM depends on a number of factors: physical parameters (σ, ν and α), the type of flow (i.e. high or low Reynolds number), discretization and delta function interpolation. Several efforts have been made to study the stability of the IBM [19, 1, 6, 7, 31, 23]. We will not break new ground in the mathematical techniques used to analyze stability but will instead extend the work of some of these authors to simulate porous flow and study its effects. Each of these existing techniques comes with inherent advantages and disadvantages. By looking at the same problem from different angles, we hope to provide a broad (but not exhaustive) overview of the methodologies and considerations in analyzing stability. The following analyses will be done in this chapter:

1. Linear stability analysis of the original continuous problem in 1D (extends the work of Stockie [29]),
2. Stability of semi-discrete equations in 1D: discrete in time only (extends the work of Stockie and Wetton [31]),
3. Timestep restrictions for the fully discrete equations (extends the work of Lai [19])

4. Linear stability of a permeable IB with a circular equilibrium shape in 2D (extends the work of Stockie et al. [7]).

The first analysis yields a dispersion relation that shows the relation of parameters for a stable solution. The next two methods yield a time step restriction for the IBM. The last approach (4) is done in 2D for a circular membrane as this is a common geometry treated in 2D simulations.

3.2 Linear Stability Analysis

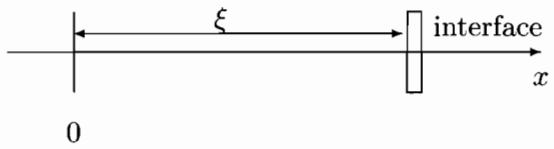

Figure 3.1: Interface position

If we want to study the influence of physical parameters alone on the stability of the porous IBM, we need to do a linear stability analysis. We obtain a dispersion relation between the physical parameters describing the fluid and IB (σ, ν and α), extending the analysis done by Stockie [29] for impermeable immersed boundaries in 1D.

3.2.1 Derivation of Dispersion Relation

Figure 3.1 shows the location of the interface or membrane $\xi(t)$[1]. ξ_0 is the equilibrium stress free position of the fiber. We follow the notation from Chapter 3 and ν is viscosity of the fluid. There is no direct analogue of equations (2.1), (2.2), (2.3) and (2.8) in 1D that contains pressure and incompressibility effects. Therefore, we instead consider a model problem consisting of the heat equation with the singular forcing term given by

$$\frac{\partial u}{\partial t} = \nu \frac{\partial^2 u}{\partial x^2} + f(\xi(t), t)\delta(x - \xi(t)). \tag{3.1}$$

The no slip condition is modified to incorporate porosity using 1D analog of (2.12) and (2.13)

$$\frac{d\xi}{dt} = u(\xi(t), t) - \alpha\sigma(\xi(t) - \xi_0). \tag{3.2}$$

[1]In Sections 3.2, 3.3 and 3.4, we have used the notation $\xi(t)$ in place of $\vec{X} = (X, Y)$ to represent the fiber location. In Section 3.5, we will use a notation for the fiber position in polar co-ordinates (X^r, X^θ).

The fiber force is given by

$$f(\xi(t),t) = -\sigma(\xi(t) - \xi_0).$$

Without loss of generality, we can translate the origin so that $\xi_0 = 0$. Eq. (3.1) can be written as two heat equation problems

$$\frac{\partial u}{\partial t} = \nu \frac{\partial^2 u}{\partial x^2} \quad \text{for} \quad x < \xi(t), \tag{3.3}$$

$$\frac{\partial u}{\partial t} = \nu \frac{\partial^2 u}{\partial x^2} \quad \text{for} \quad x > \xi(t) \tag{3.4}$$

coupled by a jump condition

$$[u_x] = u_x(\xi^+,t) - u_x(\xi^-,t) = -\frac{f(\xi(t),t)}{\nu} = \frac{\sigma\xi(t)}{\nu}. \tag{3.5}$$

After inserting $\xi_0 = 0$ in (3.2), we get

$$\frac{d\xi}{dt} = u(\xi(t),t) - \alpha\sigma\xi(t).$$

Linearizing the problem and assuming $|\xi(t)|$ and $|u(x,t)|$ to be small, we get

$$\frac{\partial u}{\partial t} = \nu \frac{\partial^2 u}{\partial x^2} \quad \text{for} \quad x < 0 \quad (\Omega^-), \tag{3.6}$$

$$\frac{\partial u}{\partial t} = \nu \frac{\partial^2 u}{\partial x^2} \quad \text{for} \quad x > 0 \quad (\Omega^+), \tag{3.7}$$

$$[u] = u(0^+,t) - u(0^-,t) = 0, \tag{3.8}$$

$$[u_x] = u_x(0^+,t) - u_x(0^-,t) = \frac{\sigma\xi(t)}{\nu}, \tag{3.9}$$

$$\frac{d\xi}{dt} = u(0,t) - \alpha\sigma\xi(t). \tag{3.10}$$

We look for a separable solution of (3.6)-(3.10), where u and ξ will be in the form of

$$u(x,t) = X(x)e^{\lambda t}, \tag{3.11}$$

$$\xi(t) = \Xi_0 e^{\lambda t}. \tag{3.12}$$

Step A: Find Ξ_0

Substituting (3.11) and (3.12) into (3.10), we get

$$\lambda \Xi_0 e^{\lambda t} = X(0)e^{\lambda t} - \alpha\sigma\Xi_0 e^{\lambda t} \Rightarrow \Xi_0 = \frac{X(0)}{\lambda + \alpha\sigma} \tag{3.13}$$

Step B: Solve for $X(x)$

Substitute (3.11) and (3.12) into both (3.6) and (3.7). In both cases, we let

$$X(x) = Ae^{\sqrt{\frac{\lambda}{\nu}}x} + Be^{-\sqrt{\frac{\lambda}{\nu}}x}$$

To ensure that we get a bounded solution as $x \to \pm\infty$, we get

$$X(x) = \begin{cases} Ae^{\beta x} & \text{if } x < 0 \\ Be^{-\beta x} & \text{if } x > 0 \end{cases} \tag{3.14}$$

where $\beta^2 = \frac{\lambda}{\nu}$ and let β be the root with a positive real part.

Step C: Determine λ

Using (3.8)

$$[u] = 0$$

$$\begin{aligned} &\Rightarrow Be^{-\beta 0} - Ae^{\beta 0} = 0 \\ &\Rightarrow A = B = X(0) \end{aligned} \tag{3.15}$$

From (3.15), (3.11) and (3.14)

$$u(x,t) = \begin{cases} X(0)e^{\lambda t + \beta x} & \text{if } x < 0 \\ X(0)e^{\lambda t - \beta x} & \text{if } x > 0. \end{cases} \tag{3.16}$$

Substituting (3.16) and (3.13) into (3.9), we get

$$\begin{aligned} -\beta X(0)e^{\lambda t} - \beta X(0)e^{\lambda t} &= \frac{\sigma X(0)e^{\lambda t}}{\lambda + \alpha\sigma} \\ \Rightarrow -2\beta &= \frac{\sigma}{\nu} \cdot \frac{1}{\nu\beta^2 + \alpha\sigma} \\ \Rightarrow 2\nu^2\beta^3 + 2\alpha\sigma\nu\beta + \sigma &= 0. \end{aligned} \tag{3.17}$$

The dispersion relation (3.17) is a cubic equation in β. Comparing it with a cubic equation of the form $ax^3 + bx^2 + cx + d = 0$, we have $a = 2\nu^2$, $b = 0$, $c = 2\alpha\sigma\nu$ and $d = \sigma$. Evaluating the discriminant

$$\begin{aligned}\Delta &= 4b^3d - b^2c^2 + 4ac^3 - 18abcd + 27a^2d^2 \\ &= 4\nu^4\sigma^2(27 + 16\mu\alpha^3\sigma).\end{aligned}$$

Because all the parameters σ, ν and α are positive, $\Delta > 0$. Hence, there will be one real and 2 complex roots. We will now proceed to isolate the physical roots and study their nature. Using cubic root finding formula, we have an expression for the roots

$$\beta_1 = s + t \tag{3.18}$$

$$\beta_2 = -\frac{1}{2}(s+t) + \frac{\sqrt{3}}{2}(s-t)i$$

$$\beta_3 = -\frac{1}{2}(s+t) - \frac{\sqrt{3}}{2}(s-t)i \tag{3.19}$$

The discriminant is

$$\Delta = \sqrt{q^3 + r^2}$$

where

$$q = \frac{3ac}{9a^2} = \frac{c}{3a} \text{ and } r = \frac{-27a^2d}{54a^3} = \frac{-d}{2a}.$$

We can show that for positive α, σ and ν, q is always positive and r is always negative. Hence,

$$s = \sqrt[3]{r + \sqrt{q^3 + r^2}}$$

$$t = \sqrt[3]{r - \sqrt{q^3 + r^2}}.$$

We analyze the nature of the term $s + t$ in (3.18)-(3.19)

$$s + t = \frac{s^3 + t^3}{s^2 + t^2 - st}.$$

It is easy to show that the numerator reduces to $2r$, which is always negative, and since $-st = q$, the denominator is always positive. Hence, $s + t$ is always negative and we can drop the real root (3.18), based on our assumption that β will have a positive real part. On

the other hand, the complex roots have a real part $s + t$, which is always positive and so these are the physical roots. Now rewrite (3.17) as

$$\beta^3 + \frac{\alpha\sigma\beta}{\nu} + \frac{\sigma}{2\nu^2} = 0. \tag{3.20}$$

As $\frac{\alpha\sigma}{\nu} \ll 1$ for physical values of α, we obtain the following asymptotic expansion for β

$$\beta \sim (-\frac{\sigma}{2\nu^2})^{\frac{1}{3}} + \frac{\alpha\sigma}{\nu}\frac{1}{3}(\frac{2\nu^2}{\sigma})^{\frac{1}{3}}.$$

3.2.2 Stability Plots

Figures 3.2, 3.3 and 3.4 plot β and λ against physical parameters (σ, α and ν) . In all the cases the asymptotic leading order solution is very close to the exact solution for the range of values that we have chosen (we have plotted the asymptotic solution only in Figure 3.2). Figure 3.2 shows that α has little effect on the behavior of both β or λ in the physical range of α (10^{-11} to 10^{-4}). Figure 3.4 and Figure 3.3 show that while increasing σ decreases the magnitude of λ ($\lambda \sim -\sigma^{\frac{2}{3}}$), increasing ν increases the magnitude of λ ($\lambda \sim -\nu^{-\frac{1}{3}}$). This is consistent with previous work that shows that increasing viscosity stabilizes the solution, and increasing stiffness destabilizes it. In general, α will tend to stabilize the solution i.e. larger negative λ. This confirms our intuition that porosity tends to stabilize the solution.

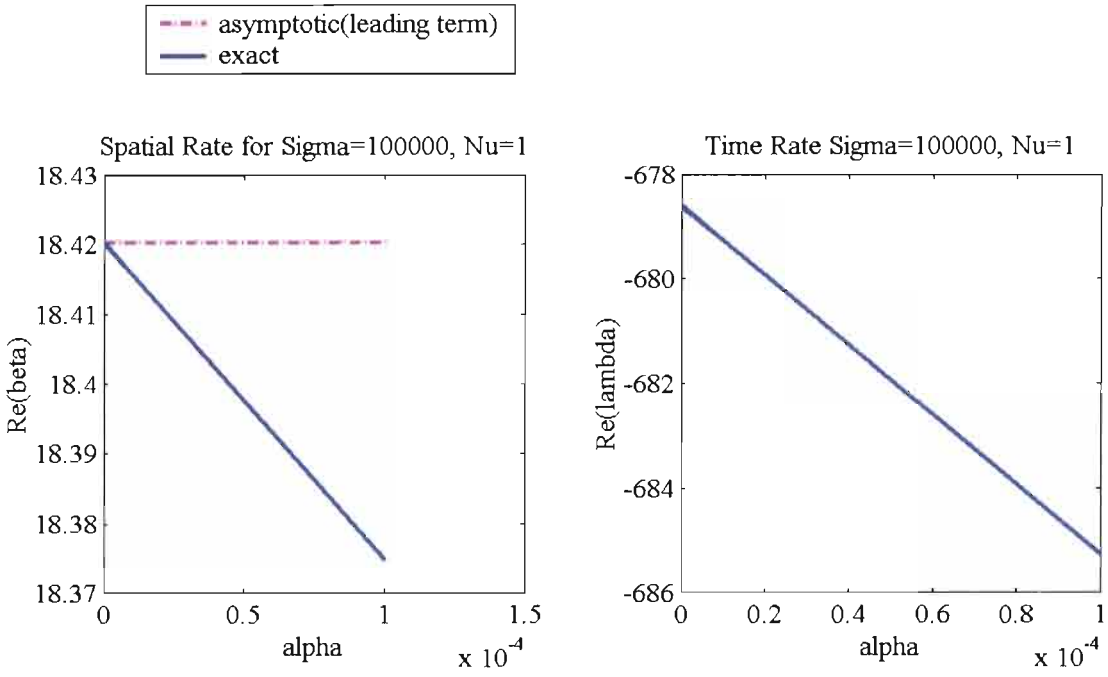

Figure 3.2: Effect of α on solution modes

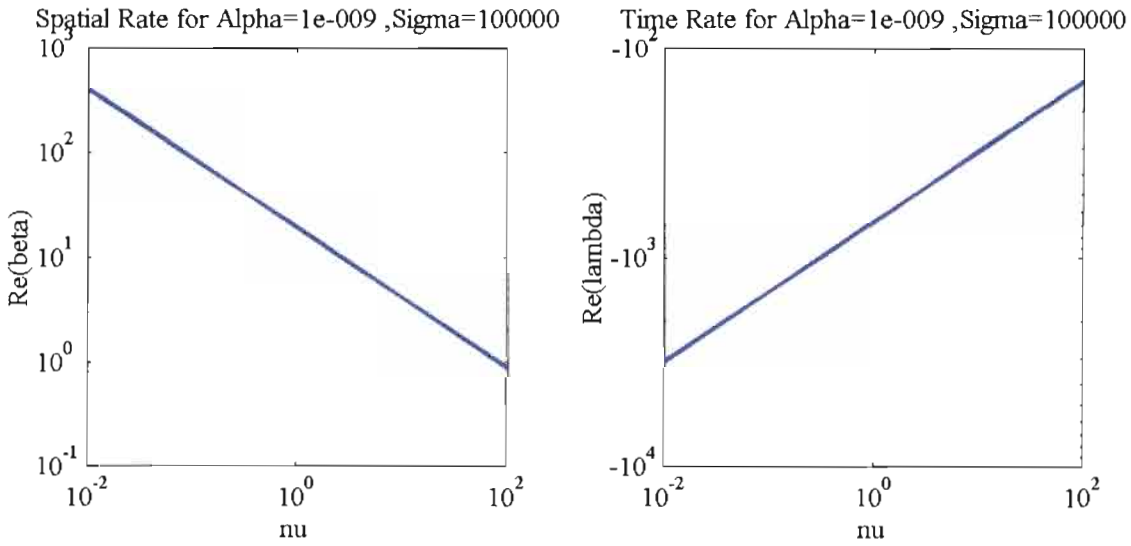

Figure 3.3: Effect of ν on solution modes

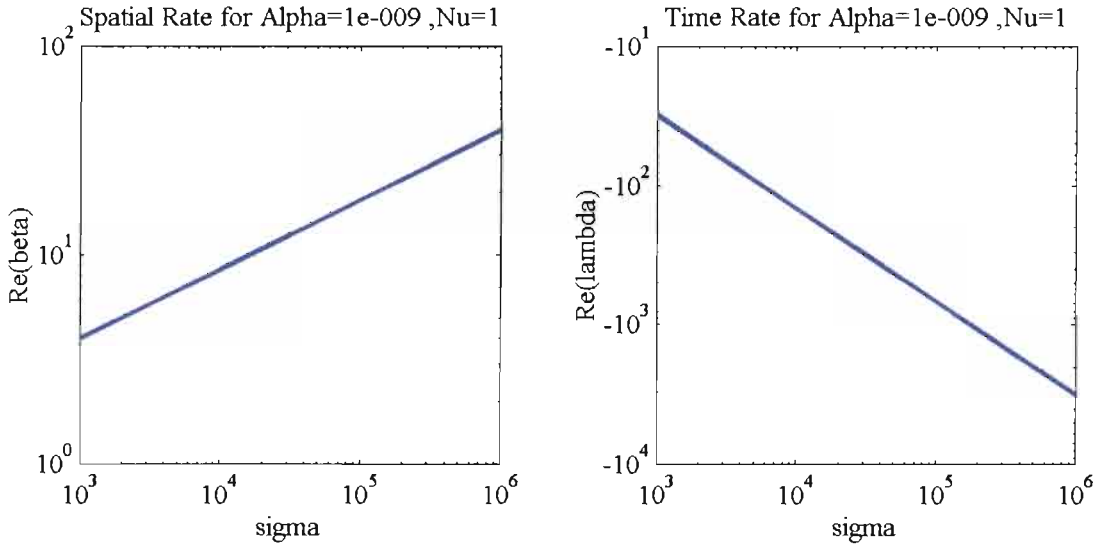

Figure 3.4: Effect of σ on solution modes

3.3 Semi-Discrete Stability Analysis

Spatial discretization plays a less important role in determining stability of the IBM than the temporal discretization [23]. We take advantage of this fact to obtain a timestep using semi-discrete stability analysis, where we discretize in time but leave the variables continuous in space.

3.3.1 Procedure

We will use the approach outlined in Stockie et al. [31] and extend it to allow for porosity. Our approach is similar to the linear stability analysis outlined in Section 3.2 with the following changes. Firstly, we use growth factors G and H to represent the factor by which the velocity and interface position respectively will grow in each timestep. Secondly, we will use a simple one sided difference to discretize the velocity and fiber positions in (3.1) and (3.2) finite differences to discretize the fluid (3.23) and fiber (3.24) velocities. Thirdly, we will consider both explicit and implicit discretization, evaluating the RHS terms either at t^n or t^{n-1}. The goal is to obtain an expression for the growth factors, and by enforcing the condition that they are less than 1 in magnitude, we can obtain a timestep restriction. Though we will use two different symbols (G and H) for the growth factors of the fluid velocities and interface position, at the conclusion of the analysis we will equate the two. This is a reasonable assumption because the fiber force alone drives the fluid velocities and so both fiber and fluid will grow /decay similarly after each timestep (we have implicitly assumed this in the linear stability analysis in Section 3.2 where we choose a common $e^{\lambda t}$ growth factor).

$$u^n(x) = G^n X^{\pm}(x) \tag{3.21}$$

$$\xi^n = H^n \xi^0 \tag{3.22}$$

$$\frac{du}{dt} = \frac{u^n - u^{n-1}}{\Delta t} \tag{3.23}$$

$$\frac{d\xi}{dt} = \frac{\xi^n - \xi^{n-1}}{\Delta t}. \tag{3.24}$$

3.3.2 Explicit Treatment

At $x = 0$, (3.21) can be written as

$$u^n(0) = G^n X(0). \tag{3.25}$$

Putting (3.25), (3.22) and (3.23) in (3.2) at $x = 0$

$$G^n X(0) - \alpha\sigma H^{n-1}\xi_0 = \frac{H^n\xi_0 - H^{n-1}\xi_0}{\Delta t}. \tag{3.26}$$

Rearranging, we get

$$\xi_0 = \frac{G^n X(0)\Delta t}{H^n - H^{n-1} + H^{n-1}\alpha\sigma\Delta t}. \tag{3.27}$$

Using (3.3) and (3.23), we get

$$\frac{u^n - u^{n-1}}{\Delta t} = \nu \frac{\partial^2 u}{\partial x^2}.$$

Using (3.21)

$$\frac{G^n X(x) - G^{n-1} X(x)}{\Delta t} = \nu G^{n-1} X_{xx}(x) \tag{3.28}$$

$$\frac{(G-1)X(x)}{\nu \Delta t} = X_{xx}(t)$$

$$X(x) = Ae^{\sqrt{\frac{(G-1)}{\nu \Delta t}}x} + Be^{-\sqrt{\frac{(G-1)}{\nu \Delta t}}x}.$$

As before, we require the solution to be bounded as $x \to \pm\infty$. Hence,

$$u(x,t) = \begin{cases} G^n A e^{\sqrt{\frac{G-1}{\nu \Delta t}}x} & \text{if } x < 0 \\ G^n B e^{-\sqrt{\frac{G-1}{\nu \Delta t}}x} & \text{if } x > 0. \end{cases} \tag{3.29}$$

The continuity condition (3.8) requires

$$B = A = X(0).$$

Substituting the expression for u into the stress jump condition (3.5), we get

$$-2\sqrt{\frac{G-1}{\nu \Delta t}} G^{n-1} X(0) = \frac{\sigma}{\nu} H^{n-1} \xi_0.$$

Using (3.27), we get

$$-2\sqrt{\frac{(G-1)}{\nu \Delta t}} = \frac{G \Delta t}{H - 1 + \alpha \sigma \Delta t} \frac{\sigma}{\nu}.$$

Let us assume that $G = H = \gamma$,

$$-2\sqrt{\frac{\gamma - 1}{\nu \Delta t}} = \frac{\gamma \Delta t}{\gamma - 1 + \alpha \sigma \Delta t} \frac{\sigma}{\nu}.$$

On expanding, we get

$$\begin{aligned} &4\nu\gamma^3 + (-12\nu + 8\nu\alpha\sigma\Delta t - \Delta t^3 \sigma^2)\gamma^2 + (4\nu\alpha^2\sigma^2\Delta t^2 - 16\nu\alpha\sigma\Delta t \\ &+ 12\nu)\gamma - 4\nu\alpha^2\sigma^2\Delta t^2 - 4\nu + 8\nu\alpha\sigma\Delta t = 0. \end{aligned} \tag{3.30}$$

This result is based on the explicit treatment of the fluid equations (3.28).

3.3.3 Implicit Treatment

For an implicit treatment of the diffusion terms (which is most common in practice) (3.28) can be rewritten as

$$\frac{G^n X(x) - G^{n-1} X(x)}{\Delta t} = \nu G^n X_{xx}(x)$$

Hence, we get in place of (3.29)

$$u(x,t) = \begin{cases} G^n X(0) e^{\sqrt{\frac{G-1}{G\nu\Delta t}}x} & \text{if } x < 0 \\ G^n X(0) e^{-\sqrt{\frac{G-1}{G\nu\Delta t}}x} & \text{if } x > 0. \end{cases} \tag{3.31}$$

Proceeding similarly, we will get the following relation

$$-2\sqrt{\frac{\gamma - 1}{\gamma\nu\Delta t}} = \frac{\gamma\Delta t}{\gamma - 1 + \alpha\sigma\Delta t}\frac{\sigma}{\nu}.$$

On expanding, we get

$$\begin{aligned}&(4\nu - \Delta t^3\sigma^2)\gamma^3 + (-12\nu + 8\nu\alpha\sigma\Delta t)\gamma^2 + (4\nu\alpha^2\sigma^2\Delta t^2 - 16\nu\alpha\sigma\Delta t \\ &+ 12\nu)\gamma - 4\nu\alpha^2\sigma^2\Delta t^2 - 4\nu + 8\nu\alpha\sigma\Delta t = 0.\end{aligned} \tag{3.32}$$

3.3.4 Growth Factor Analysis and Plots

Eqs.(3.32) and (3.30) are cubic equations in γ. For the physical range of parameters, we obtain two complex and one real root. In (3.29) and (3.31), the real part of $\sqrt{G-1}$ and $\sqrt{\frac{G-1}{G}}$ respectively needs to be positive for the solution to be bounded. Also, typical IB simulations have an oscillating decaying solution [32], a fact confirmed by the linear stability analysis in Section 3.2. Hence we reject the real root and analyze only the complex roots.

Figure 3.5, shows the growth factor contours for Δt and σ for the non -porous ($\alpha = 0$) case. In both the implicit and explicit case, the timestep decreases with increasing σ. However, for a given growth factor, the implicit case gives a larger timestep, confirming the inherent stability of the implicit scheme (the difference in timestep between the implicit and explicit scheme decreases as the growth factor approaches 1). Figure 3.6 compares the growth factor contours for Δ and σ for the non-porous ($\alpha = 0$) and porous ($\alpha = 10^{-4}, \alpha = 10^{-2}$) cases. We will assume that our algorithm (FE/ADI) will be a implicit scheme for the purposes of comparison. Timestep restrictions for the $\sigma = 10^4$ and $\sigma = 10^5$ cases are given in Table 4.6 of [32]. Our semi-discrete analysis predictions (from Figure 3.6) are very close

to the actual timestep restrictions (Table 3.1). From the almost coincident contours for the $\alpha = 0$ and $\alpha = 10^{-4}$ cases in Figure 3.6, it is clear that porosity has a negligible effect on the timestep in the physical parameter space. Figure 3.6 also shows that if we take a very large and phyiscally unrealistic porosity ($\alpha = 10^{-2}$), the timestep restriction becomes more severe. This is due to the implicit numerical scheme.

Table 3.1: Comparing the numerical and analytical timestep for the non-porous case

	From Stockie [32]	Semi-discrete analysis
$\sigma = 10^4$	7×10^{-5}	6.8×10^{-5}
$\sigma = 10^5$	10^{-5}	7×10^{-6}

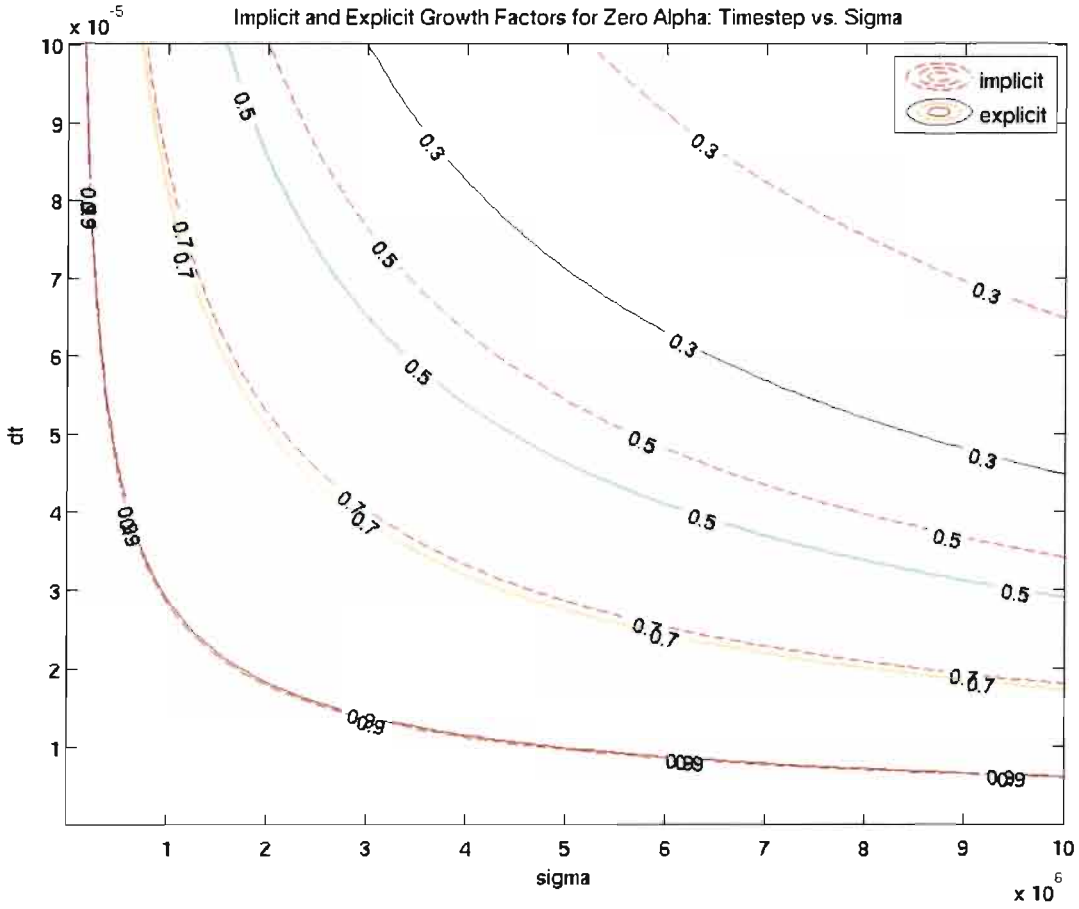

Figure 3.5: Growth factor contours for explicit/implicit treatment and $\sigma = 10^4$

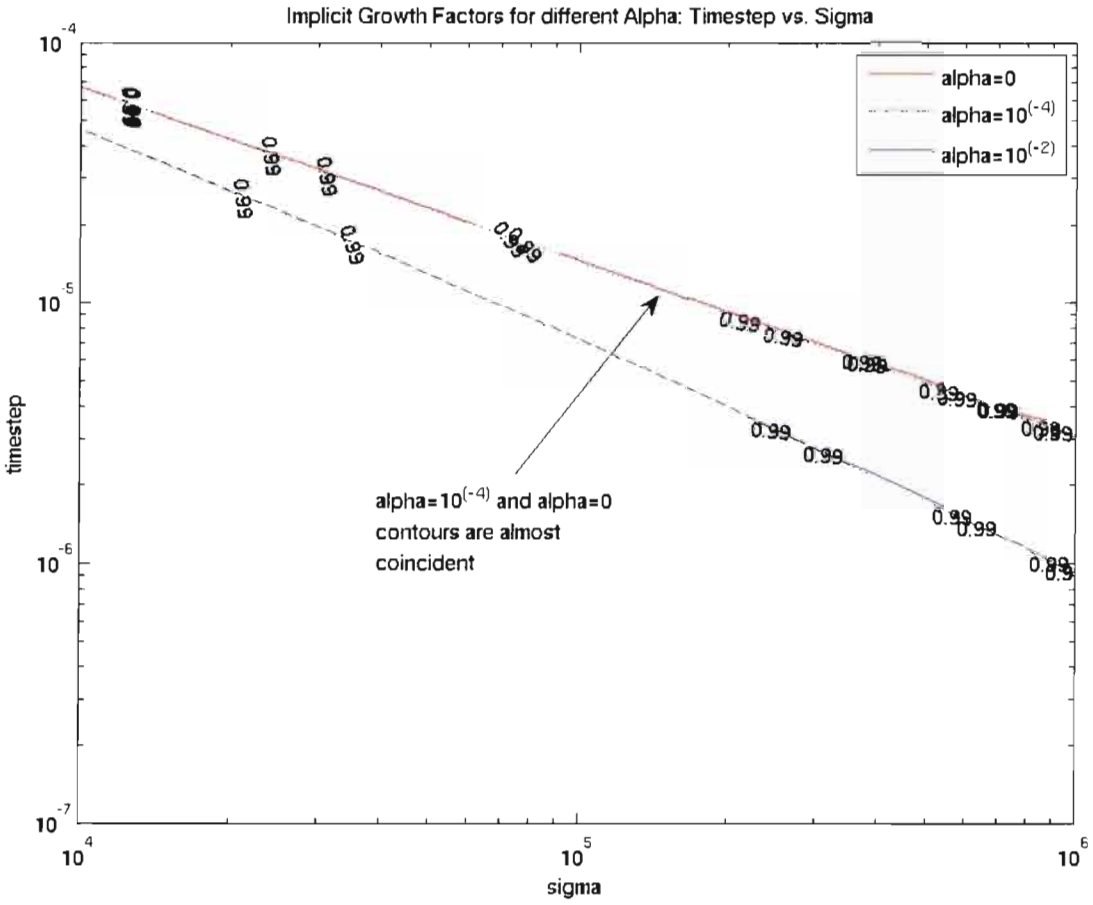

Figure 3.6: Growth factor contours for implicit treatment ($\alpha = 0$, $\alpha = 10^{-4}$ and $\alpha = 10^{-2}$)

3.4 Fully Discrete Scheme

In this section, we perform a simple analysis of the timestep restriction in the fully dicrete scheme. To this end, we extend the work of [19] (in Section L3.3, pg 19-24 [2]) to incorporate porosity. Some key aspects of this approach need to be emphasized as they are considerably different from those used in Section 3.2 and 3.3. Firstly, we discretize the fluid equations explicitly keeping in mind that it is the IB stiffness and not the usual diffusive timestep restriction that governs the choice of Δt. Secondly, we have ignored the advection term in the Navier Stokes equations in the previous analyses, while in this analysis, we will assume a linear advection term au_x with a constant advection velocity a. Lastly, so far we have used jump conditions to obtain a condition for stability. In this analysis, we will use the original IB equations in terms of delta functions. The 1D IB equations ((L3.3) and (L3.4)) are given below (we have changed the notation to be consistent with the work done in earlier sections).

$$u_t + au_x = \nu u_{xx} + f(\xi(t), t)\delta(x - \xi(t)) \tag{3.33}$$

$$\begin{aligned} \frac{d\xi}{dt} &= u(\xi(t), t) - \alpha\sigma(\xi(t) - \xi_0) && (3.34) \\ &= \int_\Omega u(x, t)\delta(x - \xi(t))dx - \alpha\sigma(\xi(t) - \xi_0). && (3.35) \end{aligned}$$

As we did in Section 3.2, without loss of generality we can take $\xi_0 = 0$.

3.4.1 Convective and Diffusive Timestep Restriction

In Section L3.3.1 of [19], Lai derives the diffusive (3.37) and convective (3.38) timestep restriction based on the following advection-diffusion equation

$$u_t + au_x = \nu u_{xx} \tag{3.36}$$

using a von Neumann stability analysis. The 'convective' timestep is named as such because it depends on the convective velocity a of the advection-diffusion equation (we use the CFL restriction to derive this condition). The 'diffusive' timestep is named as such because it is determined by the diffusive term. As (3.36) does not involve porosity, this portion of the

[2] Henceforth, we will number sections and equations from Lai [19] with a prefix L.

analysis remains the same as [19]:

$$\Delta t_D \leq \frac{(\Delta x)^2}{2\nu} \tag{3.37}$$

$$\Delta t_C \leq \frac{2\nu}{a^2}. \tag{3.38}$$

3.4.2 Membrane Timestep Restriction

Now we will proceed to derive the membrane timestep restriction, so named because it depends on the fiber stiffness σ. Discretizing (3.33) and (3.35) explicitly

$$\frac{u_j^{n+1} - u_j^n}{\Delta t} + a\frac{u_{j+1}^n - u_{j-1}^n}{2\Delta x} = \nu\frac{u_{j+1}^n - 2u_j^n + u_{j-1}^n}{(\Delta x)^2} - \sigma\xi^n\delta_h(x_j - \xi^n)$$

$$\frac{\xi^{n+1} - \xi^n}{\Delta t} = \sum_j u_j^{n+1}\delta_h(x_j - \xi^n)\Delta x - \alpha\sigma\xi^n.$$

Following Lai's analysis, we use the properties of the delta function and the triangle inequality to obtain the following inequality

$$\frac{3\sigma(\Delta t)^2}{8\Delta x} + \sigma\alpha\Delta t - 1 \leq 0$$

which can be solved for Δt

$$\frac{-\sigma\alpha - \sqrt{(\sigma\alpha)^2 + \frac{3\sigma}{2\Delta x}}}{\frac{3\sigma}{4\Delta x}} \leq \Delta t \leq \frac{-\sigma\alpha + \sqrt{(\sigma\alpha)^2 + \frac{3\sigma}{2\Delta x}}}{\frac{3\sigma}{4\Delta x}}.$$

The left hand side of the second inequality is negative, and since timestep must be positive, (3.39) reduces to

$$\Delta t_M \leq \frac{-\sigma\alpha + \sqrt{(\sigma\alpha)^2 + \frac{3\sigma}{2\Delta x}}}{\frac{3\sigma}{4\Delta x}}. \tag{3.39}$$

On taking the conjugate of the numerator and simplifying, we get

$$\Delta t_M \leq \frac{2}{\sigma\alpha + \sigma\alpha\sqrt{1 + \frac{3}{2\Delta x\sigma\alpha^2}}}$$

. We note that for large enough $2\Delta x\sigma\alpha^2$

$$\Delta t_M \approx \frac{1}{\sigma\alpha} \tag{3.40}$$

and the timestep becomes independent of the spatial discretization. Rearranging (3.39) we get

$$\Delta t_M \leq -\frac{4\alpha\Delta x}{3} + \sqrt{(\frac{4\alpha\Delta x}{3})^2 + \frac{8\Delta x}{3\sigma}} \tag{3.41}$$

Putting $\alpha = 0$ in (3.41), we get

$$\Delta t_M \leq \sqrt{\frac{8\Delta x}{3\sigma}}$$

which is the membrane timestep restriction derived in [19] for the non-porous case. Hence, (3.41), (3.38) and (3.37) are the timestep restrictions of the explicit, centered discretization of the porous IB problem.

3.4.3 Table of Timestep Restrictions

The three timestep restrictions are given in Table 3.2. The minimum of these timesteps will determine the requirement for stability. The intersection curves in the table are the curves where one kind of timestep restriction (say convective) switches to another (say membrane).

Table 3.2: Table of timestep restrictions

	Timestep Restriction
Δt_D	$\frac{(\Delta x)^2}{2\nu}$
Δt_C	$\frac{2\nu}{a^2}$
Δt_M	$-\frac{4\alpha\Delta x}{3} + \sqrt{(\frac{4\alpha\Delta x}{3})^2 + \frac{8\Delta x}{3\sigma}}$
Intersection Curves	
$\Delta t_C = \Delta t_D$	$\Delta x = \frac{2\nu}{a}$
$\Delta t_D = \Delta t_M$	$\sigma = \frac{\frac{2\nu}{\Delta x^2}}{\frac{3\Delta x}{16\nu}+\alpha}$
$\Delta t_C = \Delta t_M$	$\sigma = \frac{\frac{a^2}{2\nu}}{\frac{3\nu}{4a^2\Delta x}+\alpha}$

3.4.4 Plots

Figure 3.7, 3.8 and 3.9 plot the contours of the timestep restrictions against σ and Δx. The regions where the different timestep restrictions ((3.38), (3.37) and (3.39)) dominate are shown and the shaded region represents the "physical" zone of parameters ($\sigma = 10^2 - 10^6$ and $\Delta x = \frac{1}{32} - \frac{1}{256}$). We get the convective velocity '$a = 76$' by approximating the maximum of the average of the two velocity components over the first 20 timesteps[3]. Increasing α tends to widen the membrane region. For very large (and physically unrealistic) α, the membrane timestep becomes independent of Δx (see Figure 3.9) confirming (3.40). For the same parameters as for $\sigma = 10^4$ FE/ADI case in Table 4.6 of [32], our timestep restriction will lie in the the convective region ($\Delta t = \frac{2\nu}{a^2} = 1.7 \times 10^{-4}$). The timestep restriction given in [32] is $\Delta t = 7 \times 10^{-5}$. The timestep is in the convective region because we are doing an explicit treatment of fluid equations in this analysis. For a FE/ADI algorithm, the convective region will dominate for greater Δx greater than in the explicit case. The important result here is that, except for very large σ, for the physical range of parameters, the membrane timestep (3.41) is unlikely to determine our timestep restriction. It will most likely be determined by some combination diffusive and convective effects.

[3]This has not been clearly stated in Lai and to our knowledge has not been treated elsewhere.

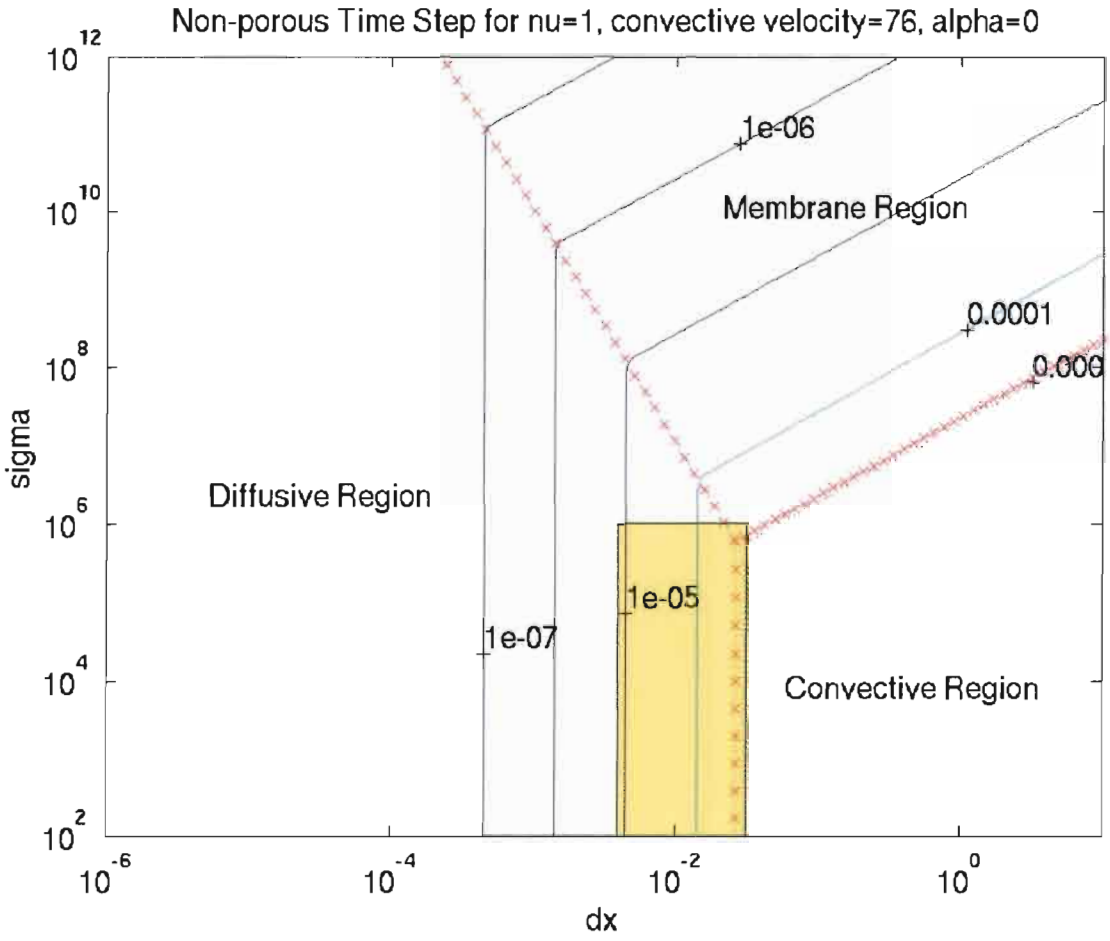

Figure 3.7: Contours of timestep for $\alpha = 0$

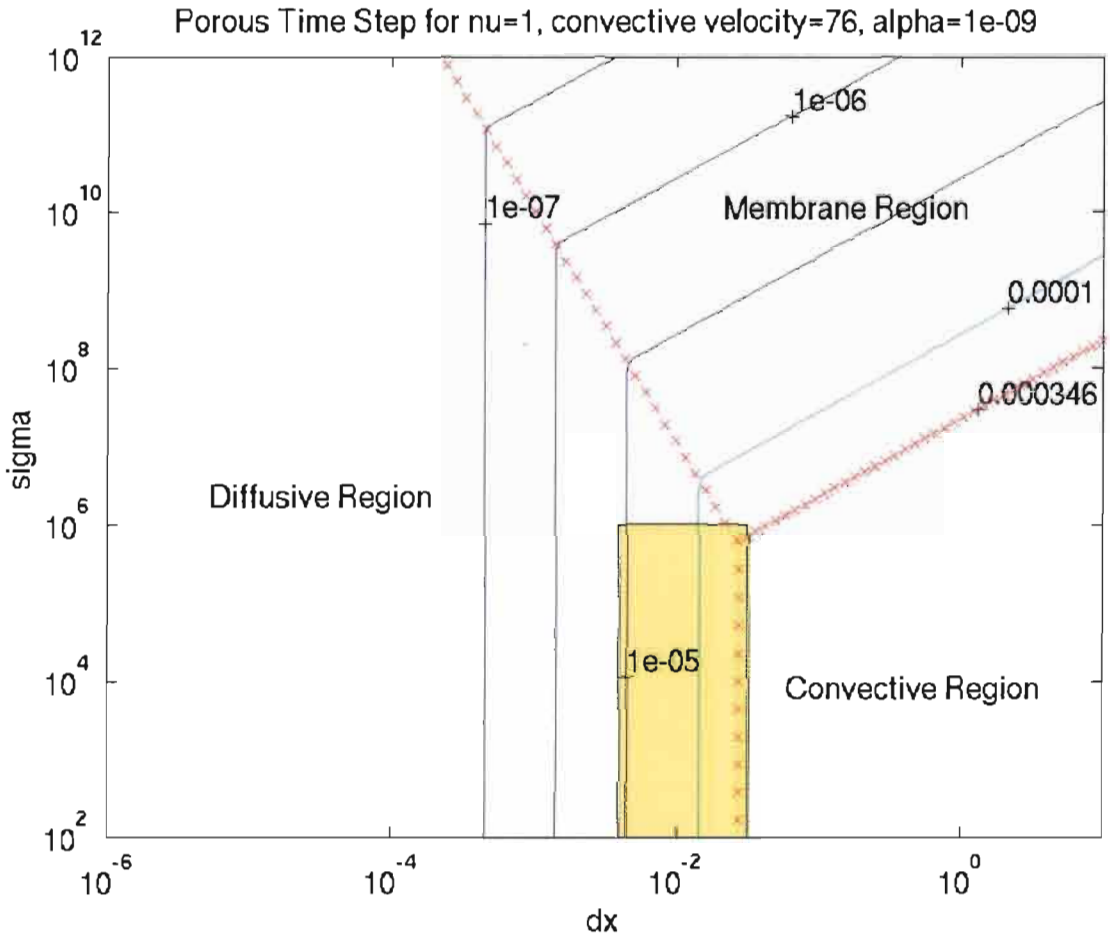

Figure 3.8: Contours of timestep for $\alpha = 10^{-9}$

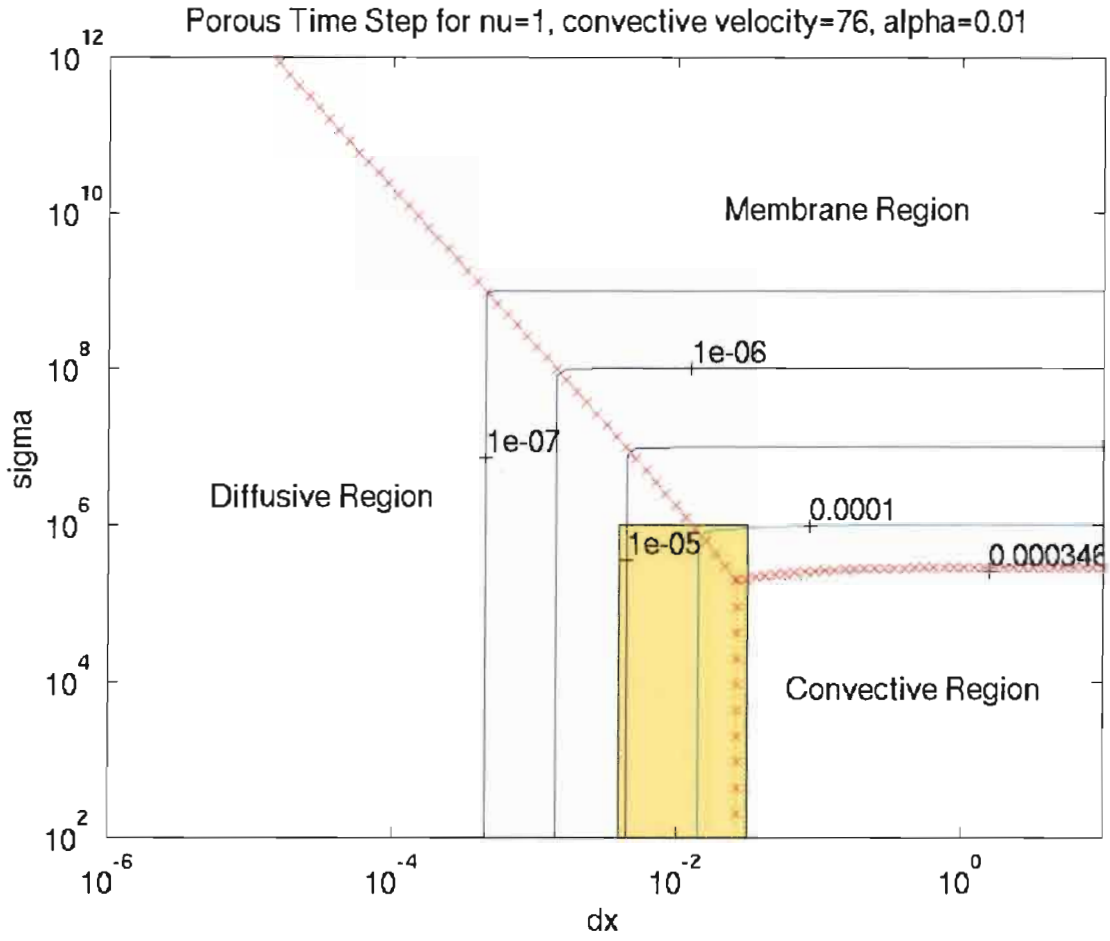

Figure 3.9: Contours of timestep for $\alpha = 10^{-2}$

3.5 Linear Stability Analysis of a 2D Circular Membrane

So far, our analysis has been primarily in 1D. The limitations of the 1D analysis are that there is no pressure or advective term in the equations (except in our extension of Lai's analysis in Section 3.4, where we have a linearized advection term). In this section we will do a 2D analysis and determine the natural modes of a circular fiber that is slightly perturbed. For this, we will extend the work of [7] to incorporate porosity. In [7], the researchers study the parametric resonance behavior of an IB in response to time-dependent internal forcing using Floquet analysis. We will do a similar analysis only this time without parametric

excitation. Instead of doing a Floquet analysis, we will study the Fourier modes of the fiber. We will broadly follow the notation in [7].

3.5.1 Small-Amplitude Approximation Equations

The procedure in [7] is to first write out the IB equations in terms of vorticity and stream function (Section P2 of [7][4]), then nondimensionalize the equations (Section P3) and obtain the small amplitude expansion (Section P4). Most of this analysis will remain as done in [7] except that we need to obtain modified $O(\epsilon)$ expressions for X_t^r and X_t^θ (in place of (P4.1c) and (P4.1d)). We assume a fiber that is slightly perturbed from a circular equilibrium state having radius $R = 1$. From (P3.3b), the fiber location can be expressed as

$$\vec{X} = \hat{r}(s) + \epsilon(X^r \hat{r} + X^\theta \hat{\theta}). \tag{3.42}$$

As we are only studying small perturbations of a circular fiber, we can assume

$$\vec{\tau} = \hat{\theta} + O(\epsilon) \approx \frac{\partial \hat{r}}{\partial s} \tag{3.43}$$

$$\vec{n} = \hat{r} + O(\epsilon) \approx -\frac{\partial \hat{\theta}}{\partial s}. \tag{3.44}$$

From (3.42), (3.43) and (3.44), we have

$$\vec{X}_s \approx \frac{\partial \hat{r}}{\partial s} + \epsilon \left(X_s^r \hat{r} + X^r \frac{\partial \hat{r}}{\partial s} + X_s^\theta \hat{\theta} + X^\theta \frac{\partial \hat{\theta}}{\partial s} \right) \tag{3.45}$$

$$= \hat{\theta} + \epsilon[(X_s^r - X^\theta)\hat{r} + (X^r + X_s^\theta)\hat{\theta}] + O(\epsilon^2). \tag{3.46}$$

Hence,

$$|\vec{X}_s| = 1 + O(\epsilon). \tag{3.47}$$

From (2.4), we get

$$\vec{F} = \frac{\partial}{\partial s}(T\tau)$$

$$= \frac{\partial T}{\partial s}\vec{\tau} + T\frac{\partial \vec{\tau}}{\partial s}. \tag{3.48}$$

Hence, we get

$$\vec{F} \cdot \vec{\tau} = -T. \tag{3.49}$$

[4]Henceforth, we will number sections and equations from paper [7] with a prefix P.

From (2.5), we get

$$T = \sigma(|X_s| - 1). \tag{3.50}$$

We will now proceed to obtain an expression for T. From (3.46)

$$\begin{aligned} T &= \sigma(|\epsilon(X_s^r - X^\theta)\hat{r} + (1 + \epsilon X^r + \epsilon X_s^\theta)\hat{\theta}| - 1) \\ &= \sigma(\sqrt{\epsilon^2(X_s^r - X^\theta)^2 + 1 + 2\epsilon(X^r + X_s^\theta) + \epsilon^2(X_s^r + X^\theta)^2)} - 1) \\ &\approx \sigma\epsilon(X^r + X_s^\theta) + O(\epsilon^2). \end{aligned}$$

From Claim 1 in [7], we find that the leading order solution of the asymptotic expansion of the vorticity and stream function is zero.
$O(1)$:

$$\xi^0 = 0$$
$$\psi^0 = 0$$

$O(\epsilon)$:

$$\begin{aligned} X_t^r\hat{r} + X_t^\theta\hat{\theta} &= \psi_\theta|_{r=1}\hat{r} - \psi_r|_{r=1}\hat{\theta} + \alpha\frac{(\vec{F}\cdot\vec{r})\hat{r}}{|\vec{X}_s|^2} \\ X_t^r &= \psi|_{r=1} - \sigma\alpha\frac{X^r + X_s^\theta}{|1 + O(\epsilon)|^2} \\ &= \psi|_{r=1} - \sigma\alpha(X^r + X_s^\theta) \qquad (3.51) \\ X_t^\theta &= -\psi|_{r=1} \qquad (3.52) \end{aligned}$$

3.5.2 Series Solution and Stability Analysis

In Section P5 of [7], the authors assume a series solution and obtain equations on either side of the fiber ((P5.4a) and (P5.4b)) and fiber evolution eqs. ((P5.4c) and (P5.4d)). Modifying the fiber evolution[5] eqs. (P5.4c) and (P5.4d) based on (3.51) and (3.52), we get

$$(\upsilon + i\eta)X_n^r = ip\psi_n(1) - \sigma\alpha(X_n^r + ipX_n^\theta) \tag{3.53}$$
$$(\upsilon + i\eta)X_n^\theta = -\psi_n'(1). \tag{3.54}$$

[5]We use the notation $\upsilon = \Lambda + i\omega$ instead of $\gamma = \alpha + i\beta$ used in [7] as we have already defined γ to be the growth factor in the semi-discrete analysis in Section 3.3, α to be the porous conductance and β to be the spatial growth rate in Section 3.2.

A change of variables in (P5.4a) results in a Bessel equation with a solution of the form

$$\xi_n = \begin{cases} b_n J_p(i\Omega_n r) & \text{if } r < 1 \\ a_n H_p(i\Omega_n r) & \text{if } r > 1. \end{cases} \tag{3.55}$$

where $\Omega_n = \sqrt{\frac{\upsilon+i\eta}{\nu}} = \sqrt{\frac{\Lambda+i\omega+in}{\nu}}$. By obtaining the corresponding stream function expressions, we get

$$\psi_n(1) = \frac{1}{2ip\Omega_n}\left[a_n H_{p-1}(i\Omega_n) + b_n J_{p+1}(i\Omega_n)\right] \tag{3.56}$$

$$\psi_n'(1) = \frac{1}{2i\Omega_n}\left[a_n H_{p-1}(i\Omega_n) - b_n J_{p+1}(i\Omega_n)\right]. \tag{3.57}$$

Using (3.53), (3.54), (3.56) and (3.57) we get expressions for X_n^r

$$\begin{aligned} X_n^r = &\frac{ip}{(\upsilon + i\eta + \sigma\alpha)}\left\{\frac{1}{2ip\Omega_n}\left[a_n H_{p-1}(i\Omega_n) + b_n J_{p+1}(i\Omega_n\right]\right\} \\ &+ \frac{ip\sigma\alpha}{(\upsilon + i\eta)(\upsilon + i\eta + \sigma\alpha)}\left\{\frac{1}{2i\Omega_n}\left[a_n H_{p-1}(i\Omega_n) - b_n J_{p+1}(i\Omega_n)\right]\right\} \end{aligned} \tag{3.58}$$

and X_n^θ

$$X_n^\theta = -\frac{1}{(\upsilon + i\eta)}\frac{\left[a_n H_{p-1}(i\Omega_n) - b_n J_{p+1}(i\Omega_n)\right]}{2i\Omega_n}. \tag{3.59}$$

We have a system of two linear equations in a_n and b_n. Taking $\upsilon + i\eta = \Omega_n^2\nu$ and solving, we get

$$a_n = \frac{\nu\Omega_n^3}{H_{p-1}(i\Omega_n)}\left[X_n^r\left(1 + \frac{\sigma\alpha}{\nu\Omega_n^2}\right) - iX_n^\theta\left(1 - \frac{p\sigma\alpha}{\nu\Omega_n^2}\right)\right] \tag{3.60}$$

$$b_n = \frac{\nu\Omega_n^3}{J_{p+1}(i\Omega_n)}\left[X_n^r\left(1 + \frac{\sigma\alpha}{\nu\Omega_n^2}\right) + iX_n^\theta\left(1 + \frac{p\sigma\alpha}{\nu\Omega_n^2}\right)\right]. \tag{3.61}$$

The jump conditions (P5.4e) and (P5.4f) with no forcing are

$$[\xi_n] = \frac{\kappa}{\nu}(p^2 X_n^\theta - ipX_n^\theta) \tag{3.62}$$

$$[\xi_n'] = -\frac{\kappa p(p^2-1)}{\nu}X_n^r. \tag{3.63}$$

Substituting (3.60), (3.61), (3.55), (3.58) and (3.59) in the jump conditions, we get

$$\begin{aligned} 0 = &i\left\{\phi\Omega_n^3\left[\frac{H_p(i\Omega_n)}{H_{p-1}(i\Omega_n)}(1 + \frac{\sigma\alpha}{\nu\Omega_n^2}) - \frac{J_p(i\Omega_n)}{J_{p+1}(i\Omega_n)}(1 + \frac{\sigma\alpha}{\nu\Omega_n^2})\right] + ip\right\}X_n^r \\ &+ \left\{\phi\Omega_n^3\left[\frac{H_p(i\Omega_n)}{H_{p-1}(i\Omega_n)}(1 + \frac{p\sigma\alpha}{\nu\Omega_n^2}) - \frac{J_p(i\Omega_n)}{J_{p+1}(i\Omega_n)}(1 + \frac{p\sigma\alpha}{\nu\Omega_n^2})\right] - ip^2\right\}X_n^\theta \end{aligned} \tag{3.64}$$

$$
\begin{aligned}
0 = i &\left\{ \phi\Omega_n^4 \left[2 - \frac{H_{p+1}(i\Omega_n)}{H_{p-1}(i\Omega_n)} - \frac{J_{p-1}(i\Omega_n)}{J_{p+1}(i\Omega_n)} \right] (1 + \frac{\sigma\alpha}{\nu\Omega_n^2}) + 2p(p^2-1) \right\} X_n^r \\
&- \phi\Omega_n^4 \left\{ \left[\frac{H_{p+1}(i\Omega_n)}{H_{p-1}(i\Omega_n)} - \frac{J_{p-1}(i\Omega_n)}{J_{p+1}(i\Omega_n)} \right] + \left[2 - \frac{H_{p+1}(i\Omega_n)}{H_{p-1}(i\Omega_n)} - \frac{J_{p-1}(i\Omega_n)}{J_{p+1}(i\Omega_n)} \right] \frac{p\sigma\alpha}{\nu\Omega_n^2} \right\} X_n^\theta .
\end{aligned} \tag{3.65}
$$

We get a 2×2 homogeneous linear system

$$
M \begin{pmatrix} X_n^r \\ X_n^\theta \end{pmatrix} = 0
$$

The above system has a non-trivial solution only if $det(M) = 0$. In [7], the authors found that the stability of the solution depends only on ϕ. From (3.64) and (3.65), it is clear that the stability of a porous formulation also depends on $\sigma\alpha$. In Figure 3.10 and 3.11 (zoom of Figure 3.10), we plot real and imaginary parts of (3.64) and (3.65) for the $p = 2$ using the following parameters $\phi = 10^{-4}, \rho = 1, \frac{\sigma}{\nu} = 10^4$, and $\alpha = 10^{-4}$. The intersections of the real (bold lines) and imaginary (dashed lines) represent the solution modes. As in [7], the numerical solutions are computed by augmenting a unit circle by a single p mode, so the fiber configuration at each timestep can be written as

$$
r(\theta, t) = 1 + \epsilon B(t) \cos(p\theta) + O(\epsilon^2)
$$

where $B(t) = e^{\alpha t}[\cos(\beta t) + \frac{\alpha}{\beta} \sin(\beta t)]$. We can estimate α and β by a least squares fit of the solution. The analytical solutions are also plotted in Figure 3.10. The numerical solutions and analytical predictions match up very well (see Figure 3.11). Once again, though we are using the maximum possible physical porosity ($\alpha = 10^{-4}$), the effect of porosity on the stability is very small. For very high levels of porosity ($\alpha = 2 \times 10^{-2}$), the stabilizing effect of porosity can be seen in Figure 3.12 and 3.13. Unfortunately, it is not possible to obtain a stable numerical solution at very high levels of porosity as the circular fiber will contract rapidly and we will run up against the CFL restriction on account of high fluid velocities. In the absence of such considerations, Figure 3.12 and 3.13 confirm the stabilizing trend. Figure 3.14, we plot the numerical and analytical solution for the following parameters: $p = 2, \phi = 0.004, \frac{\sigma}{\nu} = 5000$, and $\alpha = 0.002$. The numerical porous solution is more stable. The error between the numerical and analytical solution and the inability of the analytical solution to capture the porous effects is due to the large value of ϕ, as diffusion becomes significant in timescale runs and the dynamics are affected by periodicity [7].

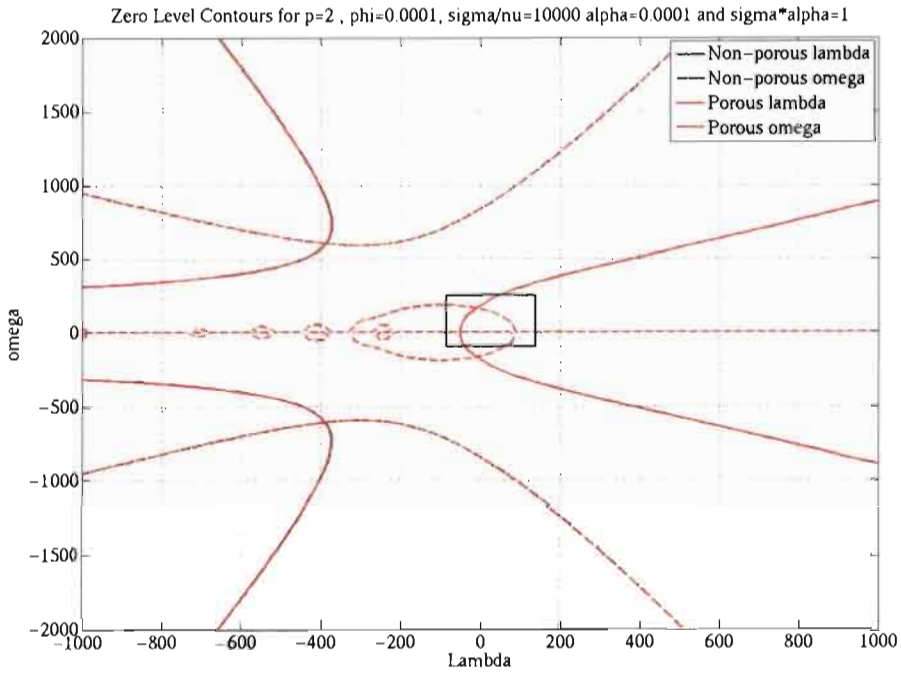

Figure 3.10: Solution modes for $p = 2, \phi = 10^{-4}, \frac{\sigma}{\nu} = 10^4$, and $\alpha = 10^{-4}$

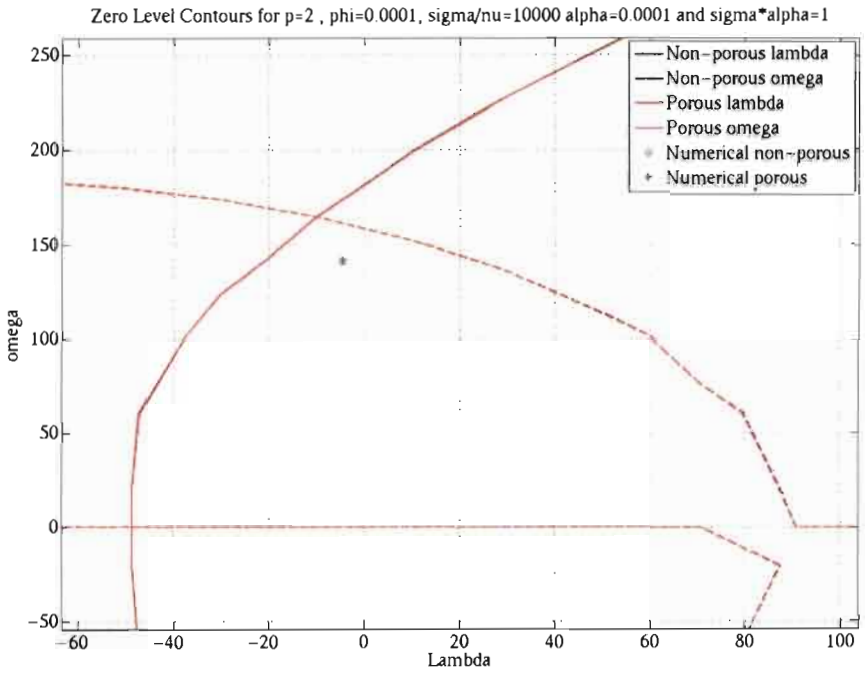

Figure 3.11: Numerical vs. analytical modes (zoom of Figure 3.10) for $p = 2, \phi = 10^{-4}, \frac{\sigma}{\nu} = 10^4$ and $\alpha = 10^{-4}$

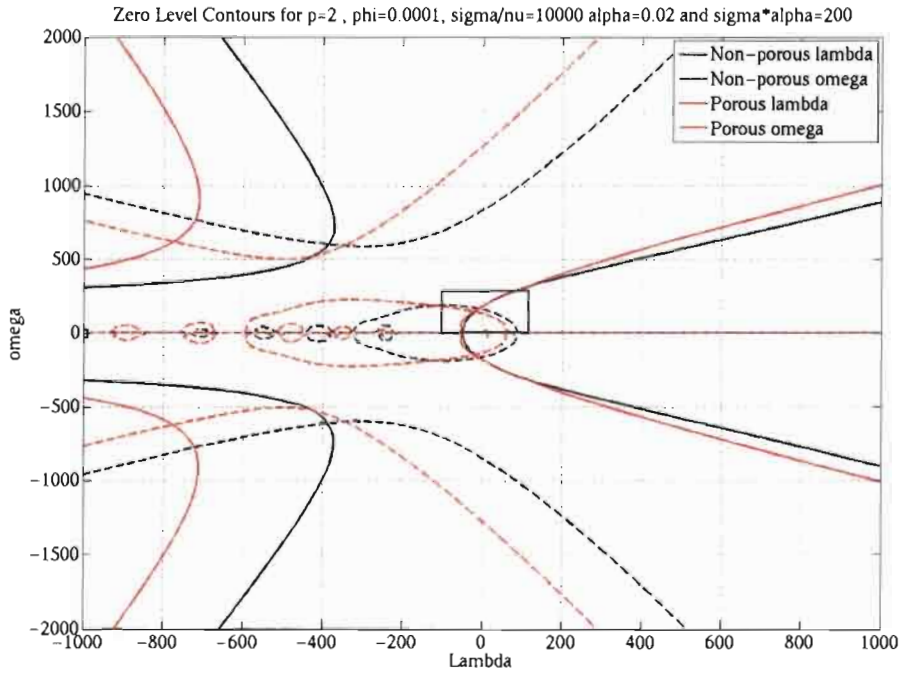

Figure 3.12: Solution modes for $p = 2, \phi = 10^{-4}, \frac{\sigma}{\nu} = 10^4$, and $\alpha = 2 \times 10^{-2}$

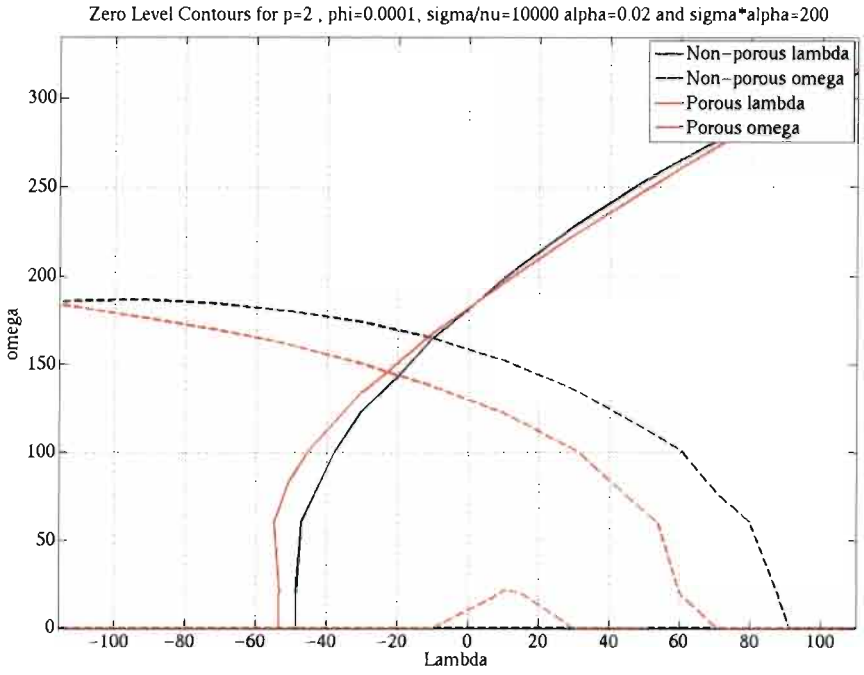

Figure 3.13: Zoom of solution modes for $p = 2, \phi = 10^{-4}, \frac{\sigma}{\nu} = 10^4$, and $\alpha = 2 \times 10^{-2}$

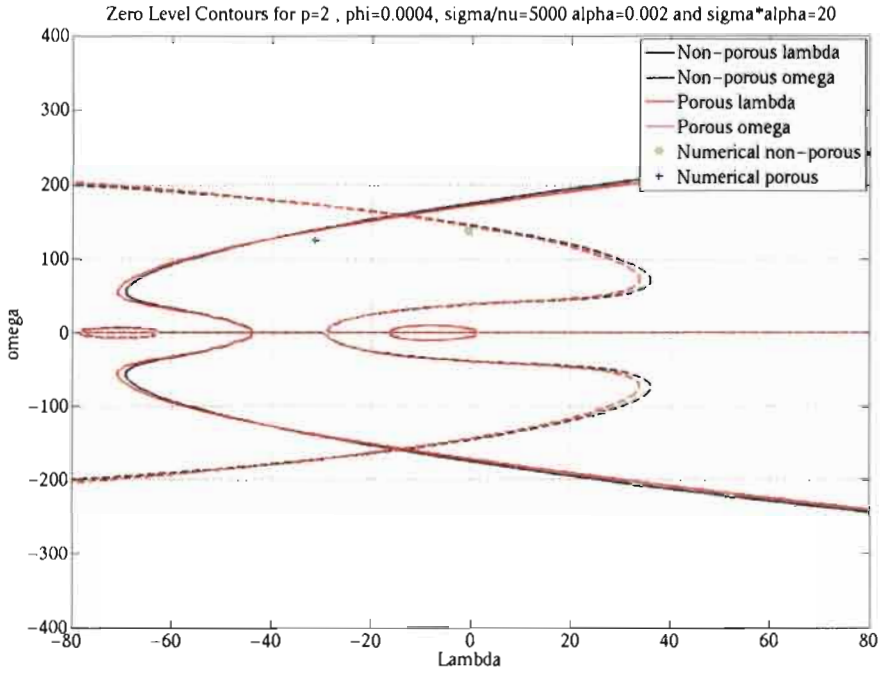

Figure 3.14: Numerical vs. analytical modes for $p = 2, \phi = 0.004, \frac{\sigma}{\nu} = 5000$, and $\alpha = 0.002$

Chapter 4

Volume Loss

4.1 Introduction

A closed, impermeable IB has a tendency to "leak fluid" through the boundary at a rate proportional to the pressure difference across the boundary. This volume loss (or more precisely, an area loss in 2D) is a consequence of numerical errors in the approximation of the divergence free condition [23], since the velocity field on the Eulerian grid is discretely divergence free, while the interpolated velocity on the Lagrangian grid is not. Peskin and Printz [24] address this problem by modifying the divergence operator for the Eulerian grid such that the velocity field will be more nearly divergence free on the Lagrangian grid also. This approach is simple to implement but is much more expensive since it widens the stencils of all the finite differences. IIM is an approach that uses modified finite difference stencils near the IB [22] in place of the delta function formulation in order to reduce the interpolation errors between fluid and fiber grids. This approach has been shown to reduce volume loss by at least an order of magnitude, but is much more complicated than the IBM, especially in 3D. A hybrid IIM/IBM approach also reduces volume loss considerably [21]. The blob projection method, developed by Cortez and Minion [5], reduces volume loss by changing the way the forces exerted by the membrane are modeled. The regularized forces are projected on onto the space of divergence free vector fields before transferring between the grids. More recently, Newren [23] developed a variation of the IB method that enforces the incompressibility constraint when transferring the velocity between the grids. His approach to conservation of volume is one of the most promising, but fails to enforce conservation of energy.

We will introduce a new method to correct volume loss which is based on the idea of directly counteracting the apparent leakage through the IB. We will henceforth call this method the "IB velocity correction." Instead of a new projection scheme [5] or finite difference stencil [24], we will directly estimate the error introduced by the delta function interpolation for the boundary velocity. For low Reynolds number Stokes flow, this error will look very similar to the porous slip velocity (we will henceforth call this the correction slip velocity to differentiate it from the porous slip velocity). This is a simple solution to the problem, requiring few changes to the algorithm and can complement other methods to reduce volume loss. We will also show that the delta function interpolation helps stabilize the standard IB method. This offers a new way of including the smoothing effect of the delta function in stability analyses.

4.2 Derivation of IB Velocity Correction

Section 2.6 discusses the delta function and its properties. In [24], using the properties of the delta function, the authors evaluate the divergence of the fiber velocity and show that differs by $O(h^2)$ from the divergence of the exact fluid velocity. We will proceed similarly, only this time to evaluate the fiber velocity itself. Using a two-dimensional Taylor series

expansion of (2.15), and suppressing the time-dependence for the moment, we have

$$\begin{aligned}
\vec{U}(X,Y) &= \sum_{\vec{x}\in Z_h^2} \vec{u}(x,y)\delta_h(x-X)\delta_h(y-Y)h^2 \\
&= \vec{u}(X,Y) \sum_{x\in Z_h} \boxed{\delta_h(x-X)h \sum_{y\in Z_h} \delta_h(y-Y)h} \quad \boxed{= 1 \text{ by (2.15)}} \\
&+ \frac{\partial \vec{u}(X,Y)}{\partial x} \cancel{\sum_{x\in Z_h} (x-X)\delta_h(x-X)h \sum_{y\in Z_h} \delta_h(y-Y)h} \quad \boxed{= 0 \text{ by (2.16)}} \\
&+ \frac{\partial \vec{u}(X,Y)}{\partial y} \cancel{\sum_{y\in Z_h} (y-Y)\delta_h(y-Y)h \sum_{x\in Z_h} \delta_h(x-X)h} \quad \boxed{= 0 \text{ by (2.16)}} \\
&+ \frac{1}{2!}\frac{\partial^2 \vec{u}(X,Y)}{\partial x^2} \boxed{\sum_{x\in Z_h} (x-X)^2\delta_h(x-X)h \sum_{y\in Z_h} \delta_h(y-Y)h} \quad \boxed{= Ch^2 \text{ by (2.15),(2.17)}} \\
&+ \frac{1}{2!}\frac{\partial^2 \vec{u}(X,Y)}{\partial y^2} \boxed{\sum_{y\in Z_h} (y-Y)^2\delta_h(y-Y)h \sum_{x\in Z_h} \delta_h(x-X)h} \quad \boxed{= Ch^2 \text{ by (2.15),(2.17)}} \\
&+ \frac{\partial^2 \vec{u}(X,Y)}{\partial x \partial y} \cancel{\sum_{x\in Z_h} (x-X)\delta_h(x-X)h \sum_{y\in Z_h} (y-Y)\delta_h(y-Y)h} \quad \boxed{= 0 \text{ by (2.16)}} \\
&+ \cdots \\
&= \vec{u}(X,Y) + \frac{Ch^2}{2}\Delta\vec{u}(X,Y) + \text{H.O.T.}
\end{aligned} \tag{4.1}$$

Ignoring higher order terms,

$$\vec{u}(X,Y) = \vec{U}(X,Y) - \frac{Ch^2}{2}\Delta\vec{u}(X,Y)$$

where $\vec{u}(X,Y)$ is the divergence free velocity at fiber location (X,Y). For a non-porous membrane, the expression (4.1) implies that the leading order error in the velocity interpolation takes the form of a slip velocity having the form

$$\vec{U_c} = \frac{Ch^2}{2}\Delta\vec{u}, \tag{4.2}$$

which we call the *correction slip velocity* because of its similarity to the porous slip velocity $\vec{U_s}$ in Section 2.4. From Section 2.6 we know that $C = 0.5$. The correction term is the Laplacian of the velocity, which suggests that the errors introduced by the velocity interpolation tend to have a stabilizing effect.

Since the fluid velocity $\vec{u}$ is defined on the fluid grid and the correction slip velocity on the fiber, $\vec{U}_c$ is actually computed by interpolating $\Delta\vec{u}$ as follows:

$$\vec{U}_c(\vec{X},t) = \frac{Ch^2}{2}\int_\Omega \Delta\vec{u}(\vec{x},t)\,\delta_h(\vec{x}-\vec{X})\,d\vec{x}.$$

The corrected fiber velocity is then given by

$$\vec{X}_t = \int_\Omega \left(1 - \frac{Ch^2}{2}\Delta\right)\vec{u}(\vec{x},t)\,\delta_h(\vec{x}-\vec{X})\,d\vec{x}.$$

In Section 4.4, we will perform simulations using this corrected fiber velocity, but first we discuss the relationship of the velocity correction to Darcy's Law.

4.3 Relation to Darcy's Law

Volume loss has been observed in previous IB simulations [24], wherein they find "a closed pressurized chamber to lose volume slowly at a rate proportional to the pressure difference across its walls, almost as though the fluid were leaking out through a porous boundary" i.e. like porous flow driven by Darcy's law. As we are primarily dealing with low Reynolds number flows here, we will explain in terms of Stokes flow why this tendency is observed. The Stokes equations are

$$\nabla p = \mu\Delta\vec{u} + \vec{f} \tag{4.3}$$

$$\nabla\cdot\vec{u} = 0. \tag{4.4}$$

Eq. (4.4) is automatically satisfied as $\vec{u}(X,Y)$ in (4.1) is divergence free. Rearranging (4.3) and multiplying by $\frac{Ch^2}{2}$

$$\frac{Ch^2}{2}\Delta\vec{u} = \frac{Ch^2}{2\mu}(\nabla p - \vec{f}).$$

This allows us to express (4.2) in terms of the IB force and pressure gradient as

$$\vec{U_c} = \frac{K_v}{\mu}(\nabla p - \vec{f}) \tag{4.5}$$

where we have defined $K_v = \frac{Ch^2}{2}$, which can be though of the "intrinsic permeability" of the IB. In our fiber material model (Section 2.2), we have assumed that tension acts only

along the fiber. Hence, if we rotate the axis such that the y-axis is perpendicular to the fiber $\vec{f} = 0$. Hence, (4.5) can be rewritten as

$$\vec{U_c} = \frac{K_v}{\mu}\frac{[p]}{a_h}\vec{n} \tag{4.6}$$

where a_h is the effective thickness that derives from the smoothing radius of the delta function [30]. From equation (4.6), it is clear that the slip velocity encompassing the leading order error due to volume loss resembles the filtration velocity given by Darcy's law for a porous membrane as shown by [30].

It is important to emphasize here that volume loss cannot be attributed to an actual leakage of fluid across the IB, since the boundary is solid. It is rather due to interpolation errors and so is a numerical phenomenon and not a physical one. Consequently, the intrinsic permeability $K_v = \frac{Ch^2}{2}$ is not a physical parameter (as in the case of the slip velocity for a porous membrane we saw in Section 2.4) but rather a numerical parameter that depends on the properties of the discretization only, namely the grid spacing h and the delta function (through C).

4.4 Simulations

Figure 4.1 plots the volume loss for an ellipse with the parameters in Table 4.1 for different levels of the grid spacing. We will scale the correction slip velocity by 0.9 as stability problems arise if we use the full velocity. Section 4.5 discusses stability issues associated with the IB velocity correction.

Table 4.1: Parameters for the numerical solution

ellipse major axis Rx	0.4
ellipse minor axis Ry	0.2
σ	10^4
ρ	1
μ	1
total time $tend$	0.02
timestep k	3.5×10^{-5}
no. of fibers N	384
grid spacing h	0.0156
fiber spacing h_b	0.005

From these simulations, we observe the following:

1. Without the IB velocity correction, decreasing the grid spacing decreases volume loss, validating equation (4.1).

2. With the IB velocity correction, volume loss decreases by anywhere between a factor of 2 and 3.

3. All cases exhibit a brief period of mild oscillations and slight volume growth before the volume starts to drop.

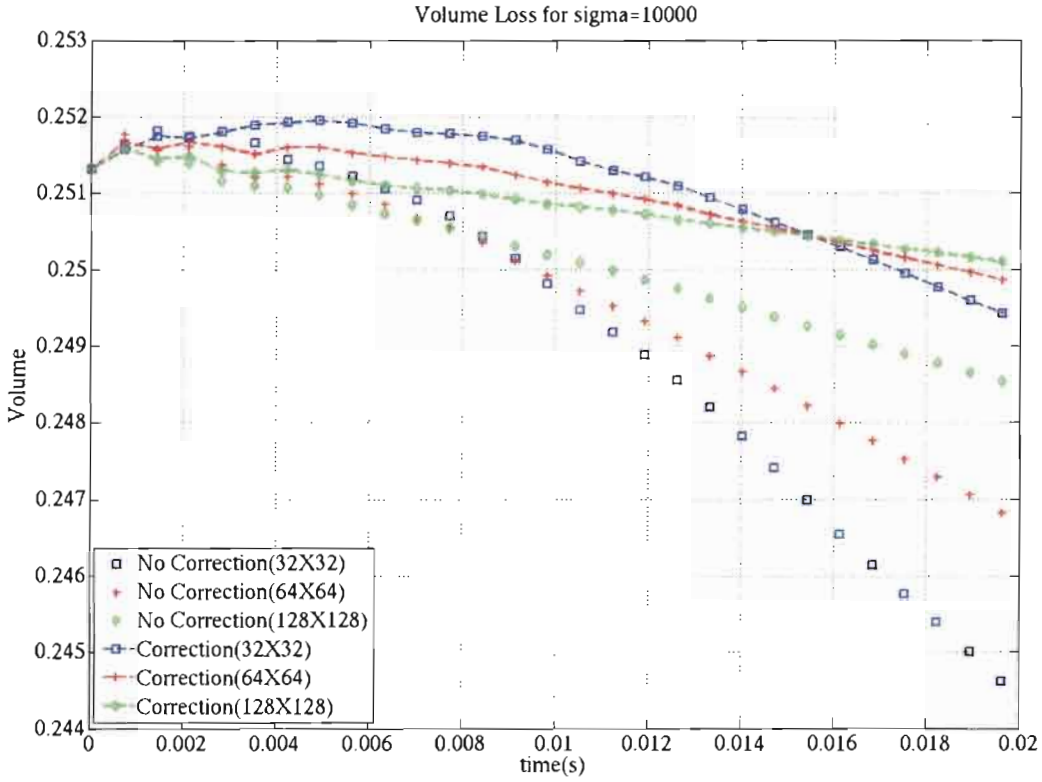

Figure 4.1: Comparing volume loss with and without second order correction terms

The reduction in volume loss by other approaches [24, 23, 5, 22] is considerably greater.

4.5 Stability

The IB velocity correction term negates the stabilizing effect of the leading order interpolation error mentioned earlier. In the simulations, we have actually had to scale the correction slip velocity in simulations by a factor of 0.9 in order to obtain a stable solution. The reason for this is that taking the full correction should in principle conserve volume, but in practice one sees a very small growth in the volume over time which leads to numerical instabilities.

An interesting corollary of this result is that the delta function has a stabilizing effect on the standard IB algorithm (i.e. without volume correction). This is not captured in the stability analysis using the jump formulation done in Chapter 3. Stockie and Wetton [31] use a smoothed delta function to capture this effect. Our IB velocity correction (4.1) could be an alternative approach.

Chapter 5

Conclusions

5.1 Contribution

The two main contributions in this work to existing body of IB research are:

1. Stability analysis of the porous IB problem proposed by Kim and Peskin [16].
2. A representation of volume loss in IBM in terms of an "intrinsic porosity" that depends on depends on fluid grid spacing (h) and the discrete delta function (δ_h).

By extending the work of others [29, 19, 7, 31] to incorporate porosity, we studied the effect of porosity on the IBM. We found that porosity has a stabilizing effect (albeit minor) on the solution. The linear stability analysis revealed that porosity leads to larger negative decay rate. The semi-discrete stability analysis revealed that porosity has minimal effect on the timestep. The fully discrete analysis revealed that among the three timestep restrictions for the explicit treatment of fluid equations (convective, diffusive and membrane), the timestep involving α and σ i.e. the membrane timestep, for the most part, is not likely to determining timestep. However, for implicit treatment of diffusion terms, the membrane timestep restriction may dominate for large σ. But once again, the effect of α is very small. The 2D linear stability analysis of a circular fiber confirmed the stabilizing effect of porosity. All the four stability analyses confirmed $\sigma\alpha$ to be the determining factor of stability.

We developed a new method for reducing volume loss called the IB velocity correction based on the porous IB formulation. The advantage of this approach is that the correction terms are in terms of $\Delta\vec{u}$ which eliminates fitting parameters required in [30] and identifies

the smoothing effect of the leading order term. It is a simple method and requires minor changes to the IB algorithm and gives between a half and a third reduction in errors due to volume loss for typical problems. We showed that, even without IB velocity correction the volume loss can be reduced by reducing the fluid grid spacing h.

5.2 Future Directions

We see several promising avenues for future research:

1. We have assumed a constant α in this work. Research could be conducted into more realistic poroelastic material models that have α as some function of $|X_s|$ based on the porous properties.

2. In our fully discrete analysis, we assumed explicit treatment of fluid equations which tends of overestimate the importance of the convective timestep restriction for the FE/ADI scheme. A fully discrete analysis with implicit diffusion could be attempted in the future. A more comprehensive study of classes of fluid problems where the convective, diffusive and membrane timestep restriction dominate needs to be conducted.

3. The counteracting effects of correction and porous slip velocities on stability needs to be studied.

4. As we have an analytical expression for volume loss in Chapter 4, we can obtain the smoothing radius of the delta function a_h described in [30]. We could conceivably use this for poroelastic material models with non-constant α.

Bibliography

[1] R. P. Beyer and R. J. LeVeque. Analysis of a one-dimensional model for the immersed boundary method. *SIAM Journal of Numerical Analysis*, 29:332–364, 1992.

[2] Richard P. Beyer. A computational model of the cochlea using the immersed boundary method. *J. Comput. Phys.*, 98(1):145–162, 1992.

[3] A. T. Chwang. A porous-wavemaker theory. *J. Fluid Mech.*, 132:395–406, 1983.

[4] R. Cortez, L. Fauci, N. Cowen, and R. Dillon. Simulation of swimming organisms: coupling internal mechanics with external fluid dynamics. *Computing in Science and Engineering*, 6(3):38–45, 2004.

[5] R. Cortez and M. Minion. The blob projection method for immersed boundary problems. *J. Comput. Phys.*, 161(2):428453, 2000.

[6] R. Cortez and D. A. Varela. The dynamics of an elastic membrane using the impulse method. *Journal of Computational Physics*, 138:224–247, 1997.

[7] Ricardo Cortez, Charles S. Peskin, John M. Stockie, and Douglas Varela. Parametric resonance in immersed elastic boundaries. *SIAM Journal of Applied Mathematics*, pages 494–520, 2004.

[8] Robert Dillon and Lisa Fauci. A microscale model of bacterial and biofilm dynamics in porous media. *Biotechnology and Bioengineering*, 68(5):536–547, 2000.

[9] Aaron L. Fogelson. A mathematical model and numerical method for studying platelet adhesion and aggregation during blood clotting. *J. Comput. Phys.*, 56:111–134, 1984.

[10] A. Gilmanov and F. Sotiropoulos. A hybrid Cartesian/immersed boundary method for simulating flows with 3D, geometrically complex, moving bodies. *Journal of Computational Physics*, 207(2):457–492, 2005.

[11] Boyce E. Griffith. *Simulating the blood-muscle-valve mechanics of the heart by an adaptive and parallel version of the immersed boundary method.* PhD thesis, New York University, 2005.

[12] T. Y. Hou. Numerical solutions to free boundary problems. *Acta Numerica*, 4:335–415, 1995.

[13] Z. J. Huang and J. M. Tarbell. Numerical simulation of mass transfer in porous media of blood vessel walls. *Amer. J. Physiol. Heart Circ. Physiol.*, 273(1):464–477, 1997.

[14] J. T. Jenkins. Static equilibrium configurations of a model red blood cell. *J. Math. Biol.*, 4:149–169, 1977.

[15] M. H. Kim and S. T. Kee. Flexible-membrane wave barrier. I: Analytic and numerical solutions. *J. Waterway, Port, Coastal, Ocean Eng.*, 122:46–53, 1996.

[16] Y. Kim and C. S. Peskin. 2-D parachute simulation by the immersed boundary method. *SIAM J. Sci. Comput.*, 28(6):2294–2312, 2006.

[17] M. C. Lai and C. S. Peskin. An immersed boundary method with formal second order accuracy and reduced numerical viscosity. *J. Comput. Phys.*, 160:705–719, 2000.

[18] M.C. Lai and C.S. Peskin. An immersed boundary method with formal second-order accuracy and reduced numerical viscosity. *Journal of Computational Physics*, 160(2):705 – 719, 2000.

[19] Ming-Chih Lai. Simulations of the flow past an array of circular cylinders as a test of the immersed boundary mehtod. *Ph.D. thesis, Courant Institute*, pages 19–24, 1998.

[20] A. T. Layton. Modeling water transport across elastic boundaries using an explicit jump method. *SIAM J. Sci. Comput.*, 28(6):2189–2207, 2006.

[21] L. Lee and R. J. LeVeque. An immersed interface method for incompressible Navier-Stokes equations. *SIAM J. Sci. Comput.*, 25(3):832–856, 2003.

[22] R. J. LeVeque and Z. Li. Immersed interface methods for stokes flow with elastic boundaries or surface tension. *SIAM J. Sci. Comput.*, 18(3):709–735, 1997.

[23] E. P. Newren. *Enhancing the Immersed Boundary Method: Stability, Volume Conservation and Implicit Solvers.* PhD thesis, University of Utah, Salt Lake City, Utah, 2007.

[24] C. S. Peskin and B. F. Printz. Improved volume conservation in the computation of flows with immersed elastic boundaries. *Journal of Computational Physics*, 105:3346, 1993.

[25] Charles S. Peskin. Flow patterns around heart valves: A numerical method. *Journal of Computational Physics*, 10:252–271, 1972.

[26] Charles S. Peskin. Numerical analysis of blood flow in the heart. *J. Comput. Phys.*, 25:220–252, 1977.

[27] Charles S. Peskin. The immersed boundary method. *Acta Numerica*, 11:479–517, 2002.

[28] S. Sivaloganathan, M. Stastna, G. Tenti, and J. M. Drake. Biomechanics of the brain: A theoretical and numerical study of Biot's equations of consolidation theory with deformation-dependent permeability. *Int. J. Nonlin. Mech.*, 40(9):1149–1159, 2005.

[29] John Stockie. A linear stability analysis for the immersed interface problem. *Unpublished Notes*, pages 4–9, 2007.

[30] John Stockie. Modelling and simulation of porous immersed boundaries. *Computers & Structures*, May 2008. Submitted.

[31] John Stockie and Brian Wetton. Analysis of stiffness in the immersed boundary method and implications for time-stepping schemes. *Journal of Computational Physics*, 151:41–64, 1999.

[32] John M. Stockie. *Analysis and Computation of Immersed Boundaries with Application to Pulp Fibers.* PhD thesis, University of British Columbia, 1997.

[33] R. Verzicco, J. Mohd-Yusof, P. Orlandi, and D. Haworth. LES in complex geometries using boundary body forces. *AIAA*, 38:427–33, 2000.

[34] R. Verzicco, J. Mohd-Yusof, P. Orlandi, and D. Haworth. Simulation of a flapping flexible filament in a flowing soap film by the immersed boundary method. *Journal of Computational Physics*, 179(2):452–468, 2002.